A&A 492, 145–162 (2008)
DOI: 10.1051/0004-6361:200809502

Astronomy & Astrophysics

The nature and evolution of Nova Cygni 2006⋆,⋆⋆,⋆⋆⋆

U. Munari[1], A. Siviero[1], A. Henden[2], G. Cardarelli[3], G. Cherini[3], S. Dallaporta[3], G. Dalla Via[3], A. Frigo[3], R. Jurdana-Sepič, S. Moretti[3], P. Ochner[3], S. Tomaselli[3], S. Tomasoni[3], P. Valisa[3], H. Navasardyan[1], and M. Valentini[4,1]

[1] INAF Osservatorio Astronomico di Padova, via dell'Osservatorio 8, 36012 Asiago (VI), Italy
e-mail: ulisse.munari@oapd.inaf.it
[2] AAVSO, 49 Bay State Road, Cambridge, MA 02138, USA
[3] ANS Collaboration, c/o Osservatorio Astronomico, via dell'Osservatorio 8, 36012 Asiago (VI), Italy
[4] Isaac Newton Group of Telescopes, Apartado de Correos 321, 38700 Santa Cruz de La Palma, Spain

Received 2 February 2008 / Accepted 8 September 2008

ABSTRACT

Aims. Nova Cyg 2006 has been intensively observed throughout its full outburst. We investigate the energetics and evolution of the central source and of the expanding ejecta, their chemical abundances and ionization structure, and the formation of dust.
Methods. We recorded low, medium, and/or high-resolution spectra (calibrated into accurate absolute fluxes) on 39 nights, along with 2353 photometric $UBVR_cI_c$ measures on 313 nights, and complemented them with IR data from the literature.
Results. The nova displayed initially the normal photometric and spectroscopic evolution of a fast nova of the FeII-type. Pre-maximum, principal, diffuse-enhanced, and Orion absorption systems developed in a normal way. After the initial outburst, the nova progressively slowed its fading pace until the decline reversed and a second maximum was reached (eight months later), accompanied by large spectroscopic changes. Following the rapid decline from second maximum, the nova finally entered the nebular phase and formed optically thin dust. We performed a photo-ionization analysis of the emission-line spectrum during the nebular phase, which showed a strong enrichment of the ejecta in nitrogen and oxygen, and none in neon, in agreement with theoretical predictions for the estimated 1.0 $M_\odot$ white dwarf in Nova Cyg 2006. The similarities with the poorly investigated V1493 Nova Aql 1999a are discussed.

Key words. stars: dwarf novae – stars: individual: V2362 Cyg

1. Introduction

Classical novae are powered by thermonuclear runaways occurring on white dwarfs in close binary systems of the cataclysmic variable type, during which H-rich material accreted from a low-mass companion is burned and explosively ejected into the interstellar medium, typically at ∼1000 km s^{-1} bulk velocity and 10^{-4} $M_\odot$ total mass. Mixing with the underlying white dwarf material affects the chemistry of the ejecta, which is dominated by non-equilibrium CNO-burning products. Classical novae are instrinsically very luminous objects (with a luminosity approaching or exceeding the Eddington luminosity for a 1 $M_\odot$ object, and M_V staying brighter than −5.5 mag for the first two weeks past maximum), and are easily observed throughout a vast fraction of our Galaxy, the Local Group, and beyond it up to the Virgo Cluster. The well-established relation between their absolute magnitude and the speed of decline makes novae useful distance indicators (e.g. Cohen 1985).

Significant research carried out in the past at the time of photographic spectroscopy to qualitatively characterize the spectroscopic evolution of novae (e.g. Payne-Gaposchkin 1957, hereafter PG57, and references therein) has led to the discovery of common paths followed by the majority of novae, irrespective of their speed class and parentship with galactic stellar populations (e.g. McLaughlin 1960, hereafter McL60). Analogous and more quantitative investigations in the era of CCD detectors are appreciably rarer due to the large amount of telescope time allocation required, expecially if observations aim to cover the entire nova outburst. Similarly, historical photographic or amateur visual lightcurves exist for many novae (e.g. Mobberley 1999; Kiyota 2004), but densely mapped, multi-band, and accurate CCD lightcurves extending from maximum to the faintest evolutionary stages are quite rare.

This paper presents new and extensive multiwavelength photometric and spectroscopic observations of Nova Cyg 2006 (=V2362 Cyg, hereafter NCyg06). It was discovered at magnitude 10.5 by Nishimura on photographic plates exposed on April 2.807 UT (as reported by Nakano 2006), while the nova was still on the rise to its maximum. Within a few hours of the discovery announcement, several spectroscopic confirmations of the nature of the nova were made, as summarized by Yamaoka (2006a). This nova is characterized by one of the most unusual photometric behaviors ever recorded for a classical nova. We investigate in detail the initial outburst, the rebrightening that occurred several months later, and the advanced decline phase. We also report photo-ionization modeling of the emission spectrum from the expanding ejecta to estimate their total mass, their chemical partition, and the temperature and luminosity of the ionizing central white dwarf, thus adding to the limited number of novae (∼30) for which such analysis has been performed.

⋆ Table 3 and Figs. 7, 8, 16–20 are only available in electronic form at http://www.aanda.org
⋆⋆ Full Table 1 is only available in electronic form at the CDS via anonymous ftp to cdsarc.u-strasbg.fr (130.79.128.5) or via http://cdsweb.u-strasbg.fr/cgi-bin/qcat?J/A+A/492/145
⋆⋆⋆ Based in part on observations obtained with the Asiago telescopes.

Table 1. Portion of Table 1, available only electronically at the CDS, to illustrate its content. The quoted error is the Poisson error and the last column provides identification of the telescope (see details in Sect. 2.1).

HJD	band	mag	err	id
... .	...	...	...	...
2454020.2807	B	11.784	0.002	*d*
2454020.2850	U	11.891	0.005	*e*
2454020.2887	V	11.611	0.002	*d*
2454020.2933	Rc	10.785	0.001	*d*
2454020.2977	Ic	10.660	0.007	*e*
2454020.2978	Ic	10.634	0.001	*d*
2454020.3067	V	11.644	0.006	*e*
2454020.3178	B	11.869	0.007	*e*
2454020.3253	Rc	10.912	0.004	*e*
2454020.3470	U	11.741	0.028	*b*
2454020.3539	B	11.909	0.022	*b*
2454020.3574	V	11.633	0.022	*b*
2454020.3577	Rc	10.817	0.012	*b*
2454020.3580	Ic	10.606	0.032	*b*
2454021.2753	Rc	10.832	0.004	*e*
2454021.2820	B	11.751	0.006	*e*
2454021.2918	V	11.570	0.005	*e*
2454021.3003	Ic	10.591	0.007	*e*
2454021.3102	B	11.723	0.002	*d*
2454021.3179	V	11.562	0.002	*d*
2454021.3183	U	11.760	0.038	*e*
2454021.3231	Rc	10.745	0.001	*d*
2454021.3283	Ic	10.593	0.001	*d*
2454021.3755	U	11.605	0.026	*b*
2454021.3824	B	11.812	0.014	*b*
2454021.3859	V	11.566	0.030	*b*
2454021.3862	Rc	10.795	0.020	*b*
2454021.3865	Ic	10.556	0.015	*b*
... .	...	...	...	...

2. Observations

2.1. Photometry

We collected (cf. Table 1) CCD and photoelectric photometry of NCyg06 with a number of telescopes, densely covering all stages of its temporal evolution. All observations were reduced against the $UBVR_CI_C$ comparison sequence presented by Frigo et al. (2006). This sequence spans a wide range in color and allows suitable transformation from the local to the standard systems. The different instruments are associated in the next paragraph to letters *a* to *g*, which are used in Table 1 and throughout the rest of the paper to identify them.

Observations were obtained with: (*a*) the Sonoita Research Observatory (SRO) 0.35-m Celestron C14 robotic telescope using BVR_CI_C Optec filters and an SBIG STL-1001E CCD camera, 1024×1024 array, 24 μm pixels $\equiv$1.25″/pix, with a field of view of $20'\times20'$; (*b*) the 0.42-m f/5.4 Newtonian telescope operated by Associazione Ravennate Astrofili Rheyta in Bastia (Ravenna, Italy), equipped with an Apogee Alta 260e CCD camera, 512×512 array, 20 μm pixels $\equiv$1.83″/pix, field of view of $16'\times16'$ and Schuler $UBVR_CI_C$ filters; (*c*) the 0.50-m f/8 Ritchey-Chrétien telescope operated on top of Mt. Zugna by Museo Civico di Rovereto (Trento, Italy) and equipped with Optec $UBVR_CI_C$ filters. The CCD is an Apogee Alta U42 2048×2048 array, 13.5 μm pixels $\equiv$0.70″/pix, with a field of view of $24'\times24'$; (*d*) the 0.30-m Meade RCX-400 f/8 Schmidt-Cassegrain telescope owned by the Associazione Astrofili Valle di Cembra (Trento, Italy). The CCD is an SBIG ST-9, 512×512 array, 20 μm pixels $\equiv$1.72″/pix, with a field of view of $13'\times13'$. The *B* filter is from Omega and the VR_CI_C filters from Custom Scientific; (*e*) the 0.13-m f/6.6 Vixen ED130SS refractor privately owned by one of us (G.C.) and operated in Trieste (Italy). It is equipped with Custom Scientific $UBVR_CI_C$ filters and a Starlight SXV-H9 CCD camera, 1392×1040 array, 6.45 μm pixel $\equiv$1.55″/pix for a field of view of $36'\times27'$; (*f*) the 0.28-m Celestron C11 telescope privately owned by one of us (S.D.) and operated in Cembra (Trento, Italy). It is used with an Optec SSP-5 photoelectric photometer and standard B, V Johnson filters; and finally (*g*) the 1.0-m Ritchey-Chrétien telescope of the US Naval Observatory, Flagstaff Station (NOFS). A Tektronix/SITe 2048×2048 thinned, backside–illuminated CCD was used. The telescope scale is 0.6763 arcsec/pixel, with a field of view of $23\farcm1\times23\farcm1$ arcmin.

The 2353 photometric measures (89 in U, 614 in B, 621 in V, 498 in R_C, and 531 in I_C) we collected on NCyg06 on 313 different nights are listed in Table 1 (available electronic only). The overall nova light-curve and color evolution are shown in Fig. 1 (see also Kimeswenger et al. 2008), using data only from instruments *a*, *d*, and *g* (Figs. 16–20, available electronic only, present the equivalent plots using all of the data in Table 1).

2.2. Spectroscopy

A journal of the spectroscopic observations we obtained on NCyg06 is given in Table 2, where a number from *1* to *10* in column seven identifies the different telescope/spectrograph configurations, described below. Reduction of all spectroscopic observations was carried out in a homogeneous way with IRAF, and involved corrections for bias, dark, and flat fields. All spectra (with the exception of the Echelle ones) were calibrated into absolute fluxes via observations on the same nights and instrumental configurations of one or more of the following spectrophotometric standard stars: HR 718, 5501, 7001, 8634, and HD 161817. On several nights, the non-photometric conditions required a shift be applied to the zeropoint of the fluxed spectra of the nova. This shift was determined by comparing the fluxes integrated over the photometric bands on the nova spectra with the corresponding fluxes from CCD photometry of the nova for the same night (or extrapolated from adjacent nights in one case). Higher resolution observations of the nova (codes *2*, *4*, *5*, *7*, *8*, *9*, and *10* in Table 2) were always accompanied by identical observations on the same night of one or more of the following stars: HD 196740, HD 209833, HD 212571. These are fast-rotating B stars with no Hα emission, and their flat, featureless continua provided an excellent reference background to record interfering absorptions by telluric H_2O and O_2.

Low and medium resolution, absolutely fluxed spectra of NCyg06 were obtained with the 0.6-m telescope of Osservatorio Astronomico G. Schiaparelli (Varese, Italy), equipped with a grating spectrograph and an SBIG ST-10XME CCD, 2184×1472 array, 6.8 μm pixel. The slit was always aligned east-west, and its projected width was kept constant to 2.0″ through the whole observing campaign. The spectrograph spatial scale is 1.0″/pix. Five different set-ups were used: 600 ln/mm grating, range 3900–7100 Å, 1×1 binning, and 1.76 Å/pix (code *1* in Table 2); 600 ln/mm grating, range 3900–7100 Å, 2 × 2 binning, and 3.52 Å/pix (code *3*); 1800 ln/mm grating, range 6200–6900 Å, 1 × 1 binning and 0.32 Å/pix (code *2*); 1800 ln/mm grating, range 6200–6900 Å, 2 × 2 binning,

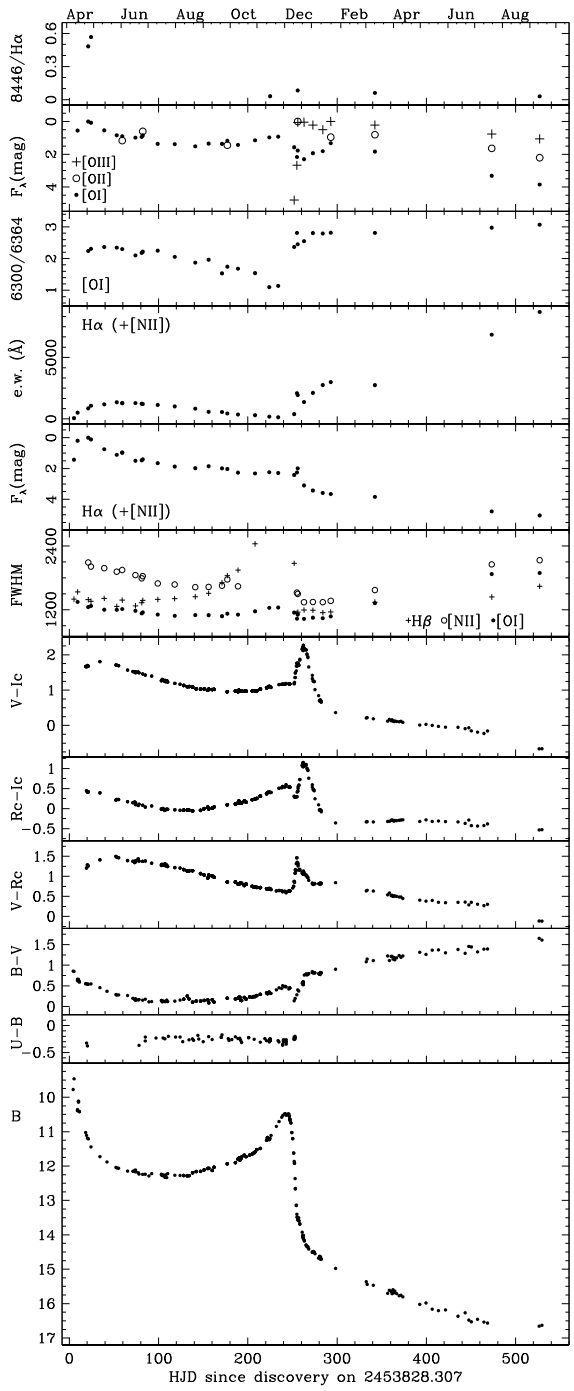

Fig. 1. *Lower six panels*: photometric evolution of Nova Cyg 2006 in the $UBVR_CI_C$ bands. *Upper six panels*: temporal evolution of [OI] 8446/Hα and [OI] 6300/[OI] 6364 flux ratios, of [OI] 6300, [OII] 7325, [OIII] 5007, and Hα integrated line flux (expressed in magnitudes relative their peak values 9.364×10^{-12}, 7.151×10^{-12}, 1.249×10^{-11}, and 3.351×10^{-10} erg cm^{-2} s^{-1}, respectively), of Hα equivalent width, and of *FWHM* (in km s^{-1}) of Hβ, [OI] 6300, and [NII] 5750 Å emission line profiles. After day +250, a growing fraction of [NII] 6548, 6584 emission contributed to the Hα flux and equivalent width.

and 0.64 Å/pix (code *4*); and 1800 ln/mm grating, range 4550−5200 Å, 2×2 binning, and 0.83 Å/pix (code *10*).

Low and medium resolution, absolutely fluxed spectra of NCyg06 were also obtained with the AFOSC imager+spectrograph mounted on the 1.82 m telescope operated in Asiago by the INAF Astronomical Observatory of Padova.

Table 2. Journal of spectroscopic observations.

date	UT	HJD	range	Å/pix	expt	S	Δt	ΔV
2006 04 08	01:44	3833.570	3900-7085	1.76	900^s	*1*	2.5	0.73
	02:56	3833.620	6175-6830	0.32	1200^s	*2*	2.5	0.73
04 12	02:07	3837.586	3900-7270	1.76	1800^s	*1*	6.5	1.64
	03:09	3837.629	6200-6800	0.32	550^s	*2*	6.5	1.64
04 13	00:21	3838.512	3600-7300	*22000*	1600^s	*5*	7.4	1.79
04 14	00:25	3839.515	3600-7300	*22000*	1600^s	*5*	8.4	1.91
04 24	00:54	3849.535	3505-7780	4.24	70^s	*6*	18.4	2.70
	01:00	3849.540	6395-7045	0.64	150^s	*8*	18.4	2.70
	01:06	3849.544	8275-9170	0.89	150^s	*9*	18.4	2.70
04 27	01:54	3852.577	3505-7780	4.23	120^s	*6*	21.5	2.89
	02:04	3852.584	6395-7045	0.64	240^s	*8*	21.5	2.89
	02:18	3852.594	8275-9170	0.89	420^s	*9*	21.5	2.89
05 11	23:12	3867.465	3850-7200	1.76	5400^s	*1*	36.4	3.44
05 25	22:31	3881.438	3800-7000	1.76	6300^s	*1*	50.3	3.74
06 01	02:01	3887.584	3495-7805	4.24	210^s	*6*	56.5	3.83
	02:11	3887.591	6390-7045	0.64	180^s	*8*	56.5	3.83
06 15	21:04	3902.378	3800-7000	1.76	1800^s	*1*	71.3	4.00
06 22	21:59	3909.417	3800-7075	3.52	5400^s	*3*	78.3	4.06
06 24	02:14	3910.595	3505-7810	4.24	160^s	*6*	79.5	4.06
	02:23	3910.600	6395-7045	0.64	270^s	*8*	79.5	4.06
07 10	21:28	3927.396	3850-7130	3.52	5400^s	*3*	96.3	4.14
07 19	00:20	3935.517	3600-7300	*22000*	6300^s	*5*	104.2	4.14
07 29	21:07	3946.382	3850-7180	3.52	5400^s	*3*	115.3	4.13
	23:09	3946.467	5980-6670	0.64	5400^s	*4*	115.4	4.13
08 21	22:28	3969.439	3850-6990	3.52	5400^s	*3*	138.3	4.04
08 31	21:21	3979.393	6000-6665	0.64	5400^s	*4*	148.3	3.99
09 05	21:26	3984.396	3830-7000	3.52	5400^s	*3*	153.3	3.96
09 20	20:52	3999.373	3850-7040	3.52	5400^s	*3*	168.3	3.83
09 26	20:53	4005.373	3505-7805	4.24	300^s	*6*	174.3	3.77
	21:11	4005.386	6395-7045	0.64	540^s	*8*	174.3	3.77
10 08	18:50	4017.287	3850-7085	3.52	3600^s	*3*	186.2	3.62
10 27	20:54	4036.373	3850-7160	1.76	3600^s	*1*	205.3	3.34
11 05	20:28	4045.354	6130-6790	0.32	3600^s	*2*	214.3	3.09
11 12	18:42	4052.280	3850-7085	1.76	3600^s	*1*	221.2	2.85
11 13	20:19	4053.280	3600-8800	*3000*	3600^s	*7*	222.2	2.81
11 22	20:02	4062.335	3840-7160	1.76	3600^s	*1*	231.2	2.32
12 10	17:33	4080.231	6190-6840	0.64	3600^s	*4*	249.1	3.78
	18:33	4080.273	3850-7055	3.52	1800^s	*3*	249.2	3.82
12 13	20:25	4083.350	3850-7055	3.52	2700^s	*3*	252.3	4.79
12 14	17:51	4084.243	3505-7580	4.24	630^s	*6*	253.1	4.94
	19:01	4084.293	3600-8900	*3000*	3600^s	*7*	253.2	4.95
12 21	18:40	4091.277	3900-7300	3.52	3600^s	*3*	260.2	5.33
	19:59	4091.332	6140-6800	0.64	2700^s	*4*	260.2	5.33
12 31	17:43	4101.237	4000-7240	3.52	3600^s	*3*	270.1	5.60
2007 01 11	18:50	4112.283	3870-7240	3.52	7200^s	*3*	281.2	5.90
01 12	18:30	4113.269	3870-7240	3.52	4500^s	*3*	282.2	5.91
01 20	17:24	4121.223	3505-7800	4.24	690^s	*6*	290.1	5.97
	18:27	4121.266	3600-8900	*3000*	1800^s	*7*	290.2	5.97
01 28	18:35	4129.272	4550-5200	0.83	5400^s	*10*	298.2	6.04
01 30	19:17	4131.301	4550-5200	0.83	7200^s	*10*	300.2	6.05
03 11	04:36	4170.683	3505-7800	4.24	1000^s	*6*	339.6	6.35
07 20	00:30	4301.523	3505-7800	4.24	6000^s	*6*	470.4	7.19
	01:48	4301.577	6395-7045	0.64	1800^s	*8*	470.5	7.20
09 14	21:50	4358.410	3505-7800	4.24	7200^s	*6*	527.3	7.01
	23:30	4358.479	6395-7045	0.64	3600^s	*8*	527.4	7.01
09 15	00:17	4358.512	8275-9170	0.89	1800^s	*9*	527.4	7.01

HJD: heliocentric Julian day (−2450000)
S: instrument identification code (detailed in Sect. 2.2)
Δt: time elapsed since maximum V brightness (April 5.6, 2006)
ΔV: decline in magnitude from maximum (V_{max}=8.0)
Fifth column: spectral dispersion, except where a slanted number is given, which indicates a resolving power (for Echelle instrumental configurations)

It is equipped with a Tektronix TK1024 thinned CCD, 1024 × 1024 array, 24 μm pixel, with a scale perpendicular to dispersion of 0.67″/pix. All observations were obtained with a 1.26″ slit always aligned east-west. Four different instrument set-ups were used: 300 ln/mm grism, range 3500−7780 Å, 1 × 1 binning, and 4.24 Å/pix (code *6* in Table 2); 1720 ln/mm volume phase holographic grism, range 6400−7050 Å, 1×1 binning, and 0.64 Å/pix (code *8*); 1280 ln/mm volume phase holographic grism, range 8270−9270 Å, 1 × 1 binning, and 0.89 Å/pix (code *9*); and the combination of a 79 ln/mm Echelle grism +150 ln/mm cross-disperser grism covering the whole wavelength range 3600−8800 Å in 13 orders with no gaps, providing a 3000 resolving power with 1 × 1 binning and 2.4″ slit width (code *7*).

High resolution spectra were obtained with the Echelle spectrograph mounted on the 1.82m Asiago telescope (code *5* in Table 2). It is equipped with an EEV CCD47-10 CCD, 1024 × 1024 array, 13 μm pixel, covering the interval $\lambda\lambda$3600−7300 Å in 32 orders (wavelength gaps between adjacent orders are

present redward of 4900 Å). The slit was always aligned east-west, and its 2″ projected width provided a 20 000 resolving power.

3. Astrometry and progenitor

Astrometry was performed on SRO images using SLALIB (Wallace 1994) linear plate transformation routines in conjunction with the UCAC2 reference catalog. Errors in coordinates were typically under 0.1 arcsec in both coordinates, referring to the mean coordinate zero point of the reference stars in each field. The coordinates we derived for NCyg06 are

$$\alpha_{J2000} = 21^{h}11^{m}32\overset{s}{.}33\ (\pm 0\overset{''}{.}12)$$
$$\delta_{J2000} = +44°48'03\overset{''}{.}74\ (\pm 0\overset{''}{.}03),$$

close to the coordinates measured by Yamaoka (2006b) at 32$\overset{s}{.}$35 (±0$\overset{''}{.}$15) and 03$\overset{''}{.}$66 (±0$\overset{''}{.}$14). The corresponding galactic coordinates are $l = 087\overset{\circ}{.}372$ and $b = -02\overset{\circ}{.}357$.

At this position, Steeghs et al. (2006) identified a faint point source on IPHAS images for Aug. 3, 2004, measured at $r' = 20.30$ (±0.05) and $i' = 19.76$ (±0.07) and with appreciable Hα emission, which they argue is the progenitor of the nova. A search of archival Asiago Schmidt plates for 1962−1984 was carried out by Jurdana-Sepič & Munari (2006) who found no brightening above the $B \sim 18.5$ plate limit. Both POSS-I and -II images also do not show a counterpart at the position of the nova.

3.1. New Asiago archive plates

In addition to the photographic plates already measured by Jurdana-Sepič & Munari (2006), we identified in the plate archives of the Asiago Schmidt telescopes another block of 57 direct-image plates covering the position of the nova progenitor over the period 1989−1997. All them have been inspected to search for a possible brightening during quiescence that could have caused the progenitor to rise above the $B \sim 18.5$ plate limit. None has been found. Table 3 (available electronic only) reports details on these plates.

To estimate the B-band magnitude expected in quiescence for the nova progenitor, we adopted the mean fluxed spectrum from Zwitter & Munari (1995) for a cataclysmic variable in quiescence, increased its reddening to match the $E_{B-V} = 0.56$ affecting NCyg06 (see Sect. 4), and scaled its flux to match the Steeghs et al. (2006) r' and i' IPHAS magnitudes. This calculation indicates that the progenitor should be $B \sim 21.0$ mag in quiescence. The negative detections on Asiago archive plates therefore exclude CV-type outbursts with an amplitude greater than $\Delta B \sim 2.5$ mag. Frequent and large amplitude outburst activity as displayed by SS Cyg ($\langle \Delta V \rangle \approx 4$ mag, outbursts every ≈55 day, of ≈15 day duration; cf. Cannizzo & Mattei 1992), a prototype cataclysmic variable, should have been easily detected on the Asiago archive plates.

3.2. The faint optical companion

Seven arcsec west of the nova lies a faint field star, identified with 2MASS 21113188+4448032 ($J = 13.716 \pm 0.029$, $H = 13.441 \pm 0.046$, $K_s = 13.480 \pm 0.037$). We measured on NOFS images for JD = 2 454 247 its optical magnitude and colors as $V = 15.22$, $U - B = +0.33$, $B - V = +0.70$, $V - R_C = +0.42$, $R_C - I_C = +0.46$, $V - I_C = +0.88$, with errors not exceeding 0.02 mag. Its astrometric position (J2000) from these images, with respect to the UCAC2 reference catalog, is $\alpha = 21\ 11\ 31.88$ (±0.1 arcsec), $\delta = +44\ 48\ 03.2$ (±0.1 arcsec). Steeghs et al. (2006) measured $r' = 14.8$ for this star, in line with our $R_C = 14.80$.

The faint optical companion could not be resolved until the advanced decline set in ∼260 days past maximum, when its contribution to the measurement of NCyg06 was no longer negligible. At later dates, the companion was spatially resolved only by instruments a and g thanks to better seeing and sampling. Photometry in Table 1 obtained with instruments b, c, d, e, and f always includes the contribution by the faint optical companion, which can be easily accounted for by using the companion's $UBVR_CI_C$ magnitudes. The photometry in Table 1 obtained with instruments a and g only includes the contribution by the faint optical companion for $t < 260$. At later dates, its was possible to measure the companion and the nova via PSF-fitting separately, and the values reported in Table 1 for $t \geq 260$ and instruments a and g pertain to the nova alone. All values quoted in the text and the light- and color-curves presented in this paper (Figs. 1, 4, 10, 15−20) have the contribution by the companion removed.

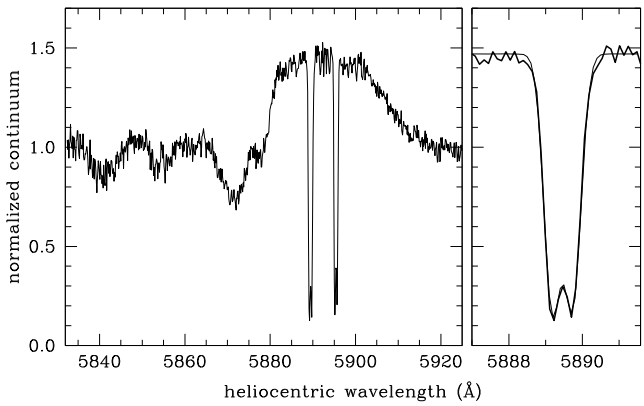

Fig. 2. *Left panel*: a small portion of the combined Echelle spectra for April 13 and 14, 2006 of Nova Cyg 2006, centered on the interstellar NaI $D_{1,2}$ absorption lines. *Right panel*: blowup of the interstellar NaI D_2 line (thicker line) showing the fit with two components at −39.1 (±0.4) and −11.1 (±0.3) km s^{-1} (thinner line).

4. Reddening

Sharp NaI $D_{1,2}$ interstellar absorption lines are prominent on the high-resolution Echelle spectra of NCyg06 obtained on April 13 and 14, 2006, close to the optical maximum. Figure 2 shows the overall appearance of the interstellar lines superimposed onto the emission component of the wide NaI P-Cyg profile of the nova itself, as well as an enlargement of their profile that reveals how the interstellar lines are actually a blend of two distinct components of similar intensity. Their heliocentric radial velocities are −39.1 (±0.4) and −11.1 (±0.3) km s^{-1}, and their equivalent widths (for the D2 component at 5890 Å) are 0.484 and 0.487 Å, respectively. Following the relation between the interstellar reddening and equivalent width of NaI D2 line calibrated by Munari & Zwitter (1997), both components correspond to a reddening of 0.28 mag, for a total reddening of $E^{TOT}_{B-V} = 0.28 + 0.28 = 0.56$, which will be adopted throughout this paper.

van den Bergh & Younger (1987) derived a mean intrinsic color $(B - V)_\circ = -0.02 \pm 0.04$ for novae at t_2. Figure 1 and the photometry in Table 1 show that NCyg06 at t_2 had $B - V = 0.54$. This corresponds to $E_{B-V} = 0.56$, a perfect match to the

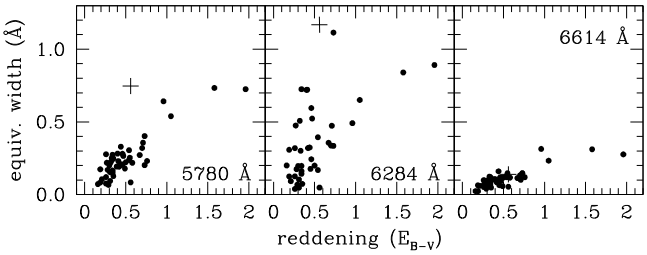

Fig. 3. Comparison between the equivalent width of three diffuse interstellar bands and interstellar reddening for field stars measured by Megier et al. (2005). The crosses represent the position of Nova Cyg 2006.

result from interstellar lines. Russell et al. (2006) preliminarily estimated $E_{B-V} = 0.59$ from infrared spectroscopy.

There are several diffuse interstellar bands (DIBs) visible on the NCyg06 spectra. On the April 8 spectra (when the continuum was strongest and smoothest), DIBs at 6203, 6270, and 6376−79 Å are present but too weak for a meaningful measure against the overlapping P-Cyg components of FeII multiplet 74 lines. DIBs at 4430, 5780, 6284, and 6614 Å show equivalent widths of 2.57, 0.75, 1.17, and 0.14 Å, respectively. A comparison of the equivalent width of the last three DIBs with the reddening/equivalent widths measured for field stars by Megier et al. (2005) is presented in Fig. 3. The correlation between reddening and DIB equivalent widths is known to be a loose one (cf. Herbig 1995). Nevertheless, it is worth noticing that, while the intensity of DIB 6614 Å in NCyg06 seems to nicely follow the mean relation for field stars, the DIBs at 5780 and 6284 are appreciably stronger than in field stars. DIB 4430 Å similarly lies above the mean relation for field stars (though still within the scatter of individual data) presented by Isobe et al. (1986). Overall, the DIBs toward NCyg06 are somewhat stronger than expected for the $E_{B-V} = 0.56$ reddening affecting the nova. The nova itself should not be contributing to the observed DIBs because their very low observed heliocentric radial velocities are what is expected for an origin in the interstellar medium and bear no relationship to the high radial velocity of the ejecta.

5. Early evolution

The early evolution of NCyg06 was that of a fairly normal FeII-type nova, from both the spectroscopic and photometric points of view, with no hint of the later peculiarities that led to one of the most peculiar lightcurves ever recorded for a nova.

5.1. Photometry

The first two months of the nova light-curve are presented in Fig. 4. The optical photometric evolution of NCyg06 was characterized by a fast rise to a maximum of $V = 8.0$ (±0.1) on Apr 5.6 (±0.5) 2006 UT (=JD 2 453 831.1). The time required to raise the final two magnitudes was $t_{r,2} \sim 2.3$ days, and the nova was discovered 2.8 days before maximum, when it was 2.5 mag fainter. A week before maximum, the nova was below the patrol plate limit at 12 mag (cf. IAUC 8698). The decline in V-band during the first two months ($4 < \Delta t < 56$, where $\Delta t = t - t_{max}$ is the time in days from maximum) strictly followed the exponential slope given by

$$V(t) = 7.6 + 2.4 \times \log(\Delta t) \quad (1)$$

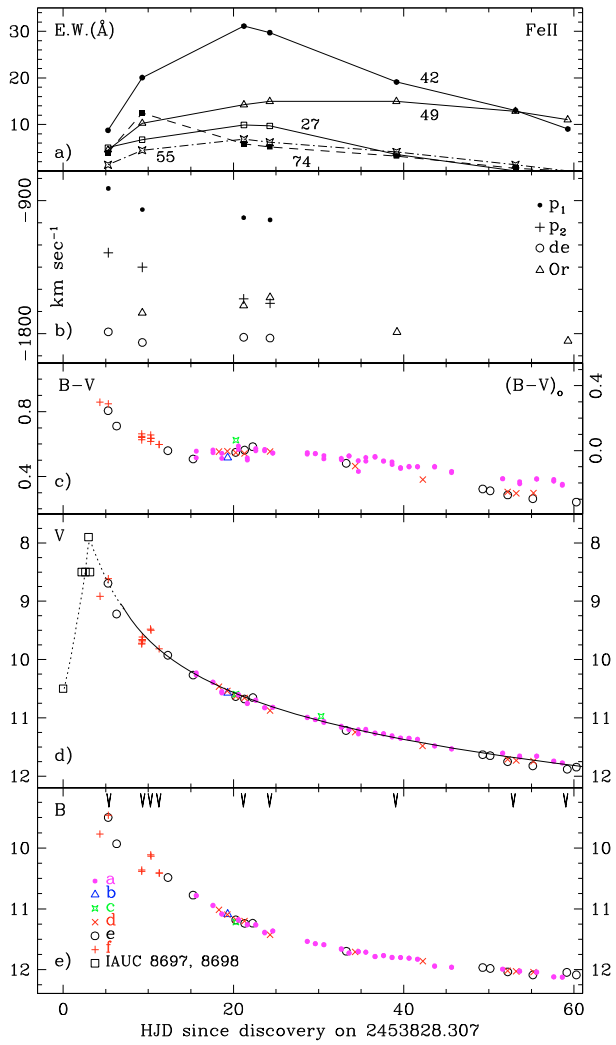

Fig. 4. The early photometric decline of Nova Cyg 2006. For instrument identification see Sect. 2.1. The solid curve over-plotted to the V data in panel **d)** is Eq. (1), while the dotted curve is drawn by hand only for eye guidance. The *a* panel shows the evolution in equivalent width of an un-blended emission line for each of the FeII multiplets 27, 42, 49, 55 and 74 (4233, 4924, 5317, 5535 and 6239 Å, respectively). Panel **b)** presents the change in radial velocity of absorption systems (the *"de"* diffuse-enhanced and the "p_1'' and "p_2'' principal systems seen in Hα, and the *"Or"* Orion system seen in HeI 6678 Å).

shown in Fig. 4 as a solid curve. A large ($\Delta B \approx 0.3$ mag) variability of NCyg06, but with constant color ($\Delta(B-V) \approx 0.0$), is superimposed on the general decline during the first ten days after maximum. This scatter cannot be ascribed to observational problems. In fact, the corresponding observations have the highest accuracy, and the results are confirmed from independent instruments, as well as repeated observations with the same instrument.

The nova decline times were $t_2^V = 10.4$ and $t_3^V = 24$ days, on the borderline between *very fast* and *fast* novae. Both t_2 and t_3 are in normal proportion among them. In fact, the following relation fits nicely the sample of ~20 best-studied novae away from the galactic Bulge (i.e. 45° ≤ galactic longitude ≤ 305°),

$$t_3 \sim 6 \times t_2^{0.7} - 7, \quad (2)$$

and NCyg06 falls right on it. The rise $t_{r,2}$ and decline t_2, t_3 times of NCyg06 are close to the proportionality relation found by

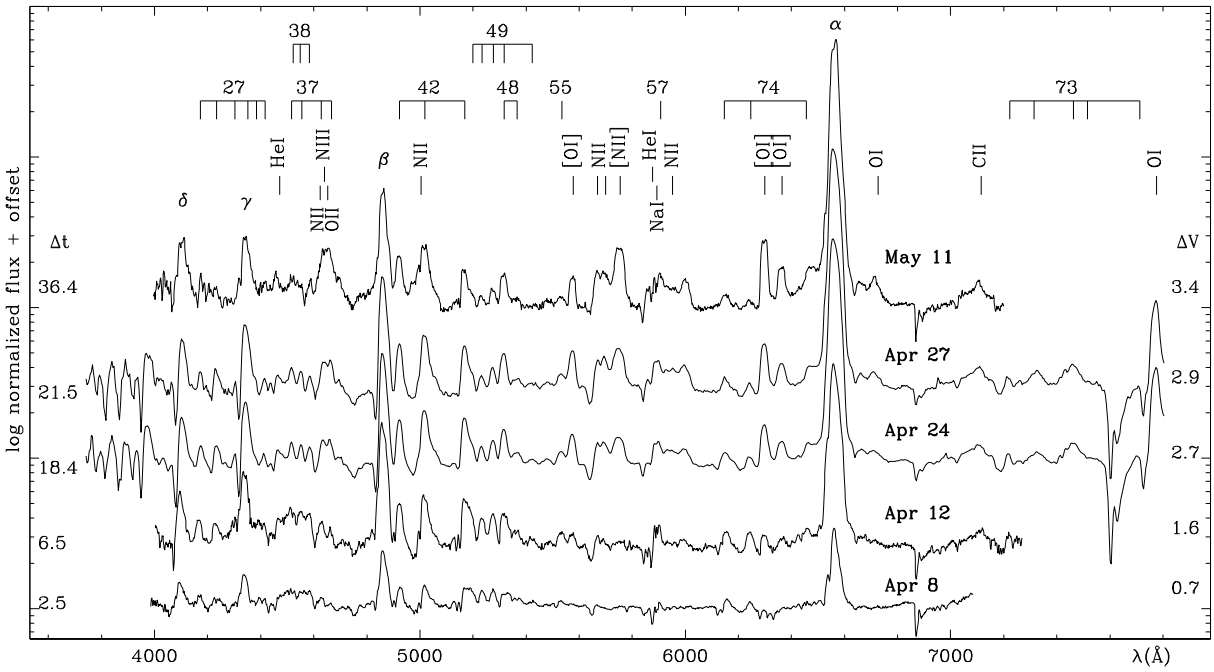

Fig. 5. Early spectroscopic evolution of Nova Cyg 2006. The spectra are continuum-normalized and shifted to avoid overlap. The ordinates are in logarithm of the flux to emphasize the visibility of weaker features. Δt and ΔV are days and magnitudes from maximum. Emission lines are identified (FeII multiplets by their numbers and comb-like markings).

Schmidt (1957): $\log t_{r,2} = -0.3 + 0.7 \log t_2 = -0.5 + 0.7 \log t_3$. In addition, the ∼13.3 mag outburst amplitude and $t_2^V = 10.4$ fall precisely on the Warner (1995) relation between amplitude and t_2.

van den Bergh & Younger (1987) found that the average intrinsic color of novae at maximum is $(B-V)_\circ = +0.23 \pm 0.06$ (dispersion 0.16 mag). Our first color measurement was obtained close to maximum at $\Delta t = +1^d.6$ (cf. Table 1). It gave $B-V = +0.85$, which corrected for the $E_{B-V} = 0.56$ reddening, corresponds to $(B-V)_\circ = +0.29$, thus reasonably close to the mean of intrinsic colors of novae at maximum.

5.2. Distance and bolometric magnitude

Both the rate of decline and the observed magnitude 15 days past maximum are popular methods of estimating the distance to the nova.

Published relations between absolute magnitude and the rate of decline generally take the form $M_{max} = \alpha_n \log t_n + \beta_n$. Given the lack of observations in B band right at maximum light, we are limited to equations valid for V band alone. Using the Cohen (1988) V–t_2 relation, the distance to NCyg06 is 8.0 kpc, and it is 7.3 kpc according to the Schmidt (1957) V–t_3 relation. Using the della Valle & Livio (1995) expression calibrated on novae appearing in the LMC and M 31, the distance to NCyg06 would increase to 9.7 kpc. Since it is not applicable to galactic novae, it will be not considered further.

Buscombe & de Vaucouleurs (1955) suggested that all novae have the same absolute magnitude 15 days after maximum light. There are several calibrations of it: $M_{15}^V = -5.2 \pm 0.1$ from Buscombe & de Vaucouleurs (1955), $M_{15}^V = -5.60 \pm 0.43$ from Cohen (1985), $M_{15}^V = -5.23 \pm 0.16$ from van den Bergh & Younger (1987), $M_{15}^V = -5.38$ from van den Bergh (1988), $M_{15}^V = -5.69 \pm 0.14$ from Capaccioli et al. (1989), $M_{15}^{pg} = -5.85$ according to Schmidt (1957), $M_{15}^{pg} = -5.50 \pm 0.18$ from de Vaucouleurs (1978), and $M_{15}^B = -5.74 \pm 0.60$ from Pfau (1976). The brightness of NCyg06 15 days after maximum light was $V_{15} = 10.45$, $B_{15} = 10.97$. Comparing with the above absolute magnitudes and correcting for $E_{B-V} = 0.56$, the distance turns out to be 6.1, 7.3, 6.2, 6.6, 7.6, 8.0, 6.8, and 7.6, respectively (approximating $m_{pg} \approx B$).

Taking the unweighted mean of the ten determinations above, the distance to NCyg06 is $d = 7.2$ kpc, with an error of the mean of 0.2 kpc and a dispersion $\sigma_d = 0.65$ kpc. The bolometric correction for an expanded photosphere with $B-V = +0.29$ is $B.C. = -0.02$ (from Drilling & Landolt 2000). Coupled with a 7.2 kpc distance, $E_{B-V} = 0.56$ and $V_{max} = 8.0$ mag, it gives for NCyg06 a bolometric magnitude at maximum of $M_{bol} = -8.0$ mag.

At NCyg06 galactic latitude, a 7.2 kpc distance translates to a height above the galactic plane of $z = 0.3$ kpc, still within the vertical scale height of the galactic Thin Disk. At galactic longitude $l = 87^\circ.37$, the line of sight to NCyg06 crosses the Perseus spiral arm 5 kpc away from the Sun, and stops midway between the Perseus and Cygnus spiral arms (cf. Vallée 2005). According to the Brand & Blitz (1993) maps, the radial velocity of interstellar matter belonging to the Perseus spiral arm where it is crossed by the line of sight to NCyg06 is ≈−40 km s^{-1}, so the −39 km s^{-1} component seen in the high-resolution profiles of interstellar NaI $D_{1,2}$ (Fig. 2 and Sect. 4) is quite possibly associated with the Perseus spiral arm. The other component at −11 km s^{-1} should be connected to material in front of the Perseus spiral arm, as suggested by the Neckel & Klare (1980) extinction maps and by the lower observed radial velocity.

5.3. Spectroscopy

The low-resolution, broad-wavelength range spectroscopic evolution of NCyg06 during the first two months of the outburst is presented in Fig. 5.

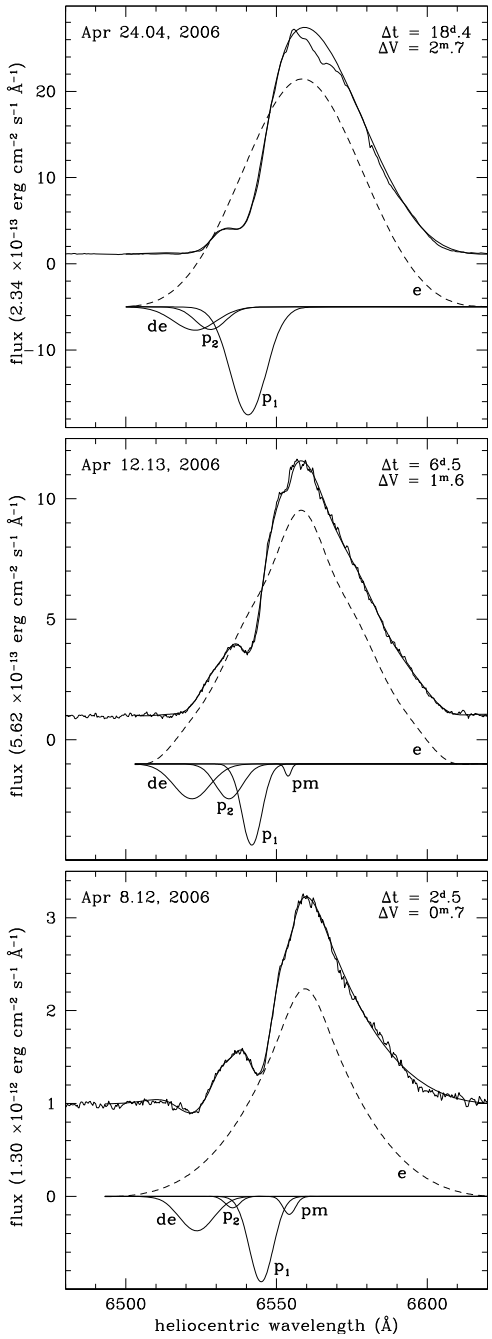

Fig. 6. Evolution of the Hα profile at three epochs during the first three weeks past maximum (see Sect. 5.3.1 for details).

5.3.1. Absorption systems

The evolution of the Hα profile during the first three weeks of the outburst is shown in Fig. 6. It is based on high-resolution observations obtained at epochs Δt = +2.5, +6.5, and +18.4 days. A fourth profile for Δt = +21.5, similar to that of day +18.4, is not shown to save space, but it is nevertheless included in Table 2, which reports the results of the Hα profile deconvolution at all four epochs. We do not consider later observations because of the reinforcement of [NII] emission in May and the blending of its 6548, 6584 Å lines with the Hα.

The Hα profile fitting was carried out assuming that the underlying emission component has a symmetric profile and that absorptions have Gaussian profiles. The profile of the emission component is therefore derived from the portion of the observed profile that extends from the peak to the asymptotic merging of the red Hα wing into the continuum. In Fig. 6 the profile of the emission component is plotted with a dashed line, those of the absorption components by solid lines.

Table 4. Heliocentric velocity, velocity span at half maximum, equivalent width, and integrated absolute flux (in units of 10^{-13} erg cm^{-2} s^{-1}) of the emission component and pre-maximum, principal and diffuse enhanced absorption systems for the Hα profiles shown in Fig. 6 (and in addition for the Hα profile of Apr 27.09, 2006 not shown in Fig. 6 to save space).

component		RV$_\odot$ (km/s)	VHM (km/s)	e.w. (Å)	F (10^{-13})
		2006, April 8.12			
emission	e	−145	1210	−89.0	1160
pre-maximum	pm	−393	95	1.00	−13
principal	p_1	−817	180	9.11	−118
	p_2	−1252	110	0.75	−10
diffuse-enhanced	de	−1788	275	5.30	−69
		2006, April 12.13			
emission	e	−220	985	−472	2655
pre-maximum	pm	−410	45	1.30	−7.3
principal	p_1	−960	150	28.1	−158
	p_2	−1310	200	16.0	−90
diffuse-enhanced	de	−1870	270	21.8	−123
		2006, April 24.04			
emission	e	−190	1050	−1280	2990
principal	p_1	−1015	270	184	−431
	p_2	−1585	230	34.0	−80
diffuse-enhanced	de	−1825	325	48.0	−112
		2006, April 27.09			
emission	e	−165	1005	−1538	3000
principal	p_1	−1030	270	207	−404
	p_2	−1595	230	35.0	−68
diffuse-enhanced	de	−1830	330	47.0	−92

The first spectrum (Δt = +2.5), obtained when the nova had already declined by ΔV = 0.7 mag, shows four absorption components, listed in Table 4. They correspond to the simultaneous presence of the classical *pre-maximum*, *principal*, and *diffuse-enhanced* absorption systems (indicated by *pm*, *p*, and *de* in Fig. 6, respectively), which are common to most novae and are described in detail by McLaughlin (1960, hereafter McL60). A noteworthy characteristic of NCyg06 is the splitting of the *principal* absorption spectrum into two components (p_1, p_2), as seen previously in other novae (e.g. N Aql 1918 and N Gem 1912). At ΔV = 0.7 mag, the *pre-maximum* absorption system was already declining in equivalent width, while the *principal* system was rapidly gaining strength and the *diffuse-enhanced* system had just emerged. Their heliocentric radial velocity, velocity width at half intensity and integrated absolute flux are given in Table 4.

Data summarized by McL60 show a correlation between *mean* radial velocity of the various absorption systems and the speed class of the nova (*mean* velocity because the velocity of any given system usually changes with time). This correlation states $v_{\rm pre-max} \approx -4750/t_2$ for the *pre-maximum* absorption system. The t_2 = 10.4 days for NCyg06 would correspond to −450 km s^{-1}, close to the observed −400 km s^{-1}

(Table 4). The velocity relation for the *principal* system is $\log v_{\rm prin} = 3.70-0.5\log t_3 = 3.57-0.5\log t_2$, and predicts ≈ -1080 km s^{-1} for NCyg06. The epoch means of the p_1,p_2 velocities in Table 4 (weighted according to their equivalent widths) are −850, −1087, −1103, and −1112 km s^{-1}. Their global average is −1040 km s^{-1}, again close to predictions. The McL60 relation for the *diffuse enhanced* system is $\log v_{\rm dif-enh} = 3.81-0.4\log t_3 = 3.71-0.4\log t_2$, and it predicts ≈ -1880 km s^{-1} velocity for NCyg06, in good agreement with the averaged observed value of −1830 km s^{-1}.

All three absorption systems in NCyg06 appear to move ∼50 km s^{-1} more slowly than predicted on the basis of the relations by McL60. The difference is actually more than twice as large. In fact, the component of the radial velocity due to the galactic rotation can be written as

$$RV_\odot = w_\circ \sin b + u_\circ \cos l \cos b - v_\circ \sin l \cos b - 2\left[A(R-R_\circ)+\alpha(R-R_\circ)^2\right] \sin l \cos b \quad (3)$$

where $R^2 = R_\circ^2 + d^2 - 2R_\circ d\cos l$, $A = -(R_\circ/2)(\mathrm{d}\omega/\mathrm{d}R)_{R_\circ}$ and $\alpha = -(R_\circ/4)(\mathrm{d}^2\omega/\mathrm{d}R^2)_{R_\circ}$. Here, R and $R_\circ$ are the nova and Sun galacto-centric distances, d is the nova-Sun distance, (l,b) the nova galactic coordinates and $(u_\circ, v_\circ, w_\circ)$ is the solar motion vector. Adopting $(u_\circ, v_\circ, w_\circ)$ = (10.0,5.3,7.2) km s^{-1} from Dehnen & Binney (1998), and $A = 17.0 \pm 1.5$ km s^{-1} kpc^{-1} and $\alpha = -2.0 \pm 0.6$ km s^{-1} kpc^{-2} from Hron (1987), the radial velocity of NCyg06 expected from galactic rotation would be −69 km s^{-1}. Therefore, it seems that the mean *barycentric* outflow velocity of the pre-maximum, principal and diffuse-enhanced spectra of NCyg06 are about 120 km s^{-1} slower than predicted by the McL60 relations.

The FeII line profiles in the low-resolution spectra for April 8 and 12 in Fig. 5, and the Echelle spectra for April 13 and 14, also show the presence of the principal and diffuse-enhanced absorption systems. The pre-maximum system had become too weak to be detected on the FeII lines by the time of the Echelle spectra. The radial velocities of the absorption systems on the FeII lines were close to what was measured for Hα. On the low-resolution April 8 spectrum, they were ≈ -830 for p_1 principal and ≈ -1700 km s^{-1} for diffuse-enhanced. On the Echelle spectrum for April 12 they were ≈ -985 for p_1 principal, ≈ -1295 for p_2 principal, and ≈ -1780 km s^{-1} for diffuse-enhanced. Also the ratio of the equivalent widths of p_1 and diffuse-enhanced was similar in Hα and FeII lines: 1.29 and 1.30, respectively, on April 12. The only major difference with Hα was in the much weaker intensity in the FeII lines of the p_2 system compared with the p_1 system.

The time behavior of the radial velocity of p_1, p_2 principal and diffuse-enhanced absorptions on the Hα profile is illustrated in Fig. 4. The velocity of the p_1 system has been increasing with time as $v_1 \propto -215\log(\Delta t)$, and for p_2 as $v_2 \propto -400\log(\Delta t)$ km s^{-1}. The velocity increase was minimal for the pre-maximum absorptions, while there has been no increase at all in the diffuse-enhanced systems. This agrees with what is seen in most novae (cf. McL60).

Feeble traces of the emergence of the *Orion* absorption system appear on the April 12 spectrum ($\Delta t = +6.5$, $\Delta V = 1.6$ mag) of Fig. 5. The Orion absorptions grew much stronger on the April 24 and 27 spectra ($\Delta t = +20$, $\Delta V = 2.8$ mag). It was still weakly present on the May 11 spectrum ($\Delta t = +36$, $\Delta V = 3.4$ mag). The Orion system affected the HeI, NII and OII lines but not the hydrogen ones, as is common in many novae. The radial velocity and equivalent width of the Orion absorption component of HeI 6678 Å are listed in Table 5, while Fig. 4 shows its velocity progression in comparison with the other absorption systems. In many novae, the velocity of the Orion absorption is comparable to or higher than for the diffuse-enhanced system, while the Orion system moves about 250 km s^{-1} slower in NCyg06.

Table 5. Radial velocity and equivalent width of the Orion absorption system as observed in the HeI 6678 Å line.

Δt (days)	ΔV (mag)	rad.vel. (km/s)	E.W. (Å)
6.5	1.6	−1660	1.6
18.4	2.7	−1610	11.0
21.5	2.9	−1555	10.0
36.4	3.4	−1790	2.3
56.5	3.8	−1850	0.8

In typical novae, as the numerous NII and OII lines of the Orion system fade away, a pair of NIII absorption lines emerges at 4097 and 4103 Å. This also occurred in NCyg06, for which the NIII absorption is quite visible on the blue wing of the Hδ emission line of the June 1 spectrum ($\Delta t = +56$, $\Delta V = 3.8$ mag) illustrated in Fig. 9. Its velocity is ≈ -2200 km s^{-1}. The June 1 spectrum corresponds to the date when the nova abandoned the exponential decline of Eq. (1), began to slow its decline rate toward the plateau phase of mid 2006 and then rose to the second maximum of late 2006. This anomalous photometric behavior was mirrored by an initially slowed, and then aborted, spectroscopic evolution. In fact, by the time the NIII 4100 Å absorption appears, a typical nova is entering the transition phase, when its spectrum turns from the stellar to the nebular type. This did not happen in NCyg06. It did not go through the transition phase and the development of the NIII absorption soon stopped. The equivalent width of the latter, in fact, reached a modest 1.1 Å on the June 1 spectrum and did not rise to the expected ∼10× larger equivalent width it should have attained at later dates. Instead, it rapidly faded away, leaving no obvious trace on the June 22 spectrum in Fig. 9.

5.3.2. Emission lines

Figure 5 shows the evolution of the emission lines during the first two months of the outburst. On $\Delta t = +2.5$, the emission lines were essentially restricted to the hydrogen Balmer series and emerging FeII lines (principally from the multiplets 42, 49, and 74), on top of a poorly structured, relatively cool continuum. The intrinsic color at that time, $(B-V)_\circ = +0.29$, was still only marginally perturbed by emission lines and corresponded to that of an A9/F0 III star. The emission line spectrum was typical of the *FeII*-class defined by Williams (1992). The expansion velocity (corrected for instrumental resolution) derived from the width at half maximum was similar for all hydrogen Balmer emission lines and amounted to 780 km s^{-1}; the velocity estimated from the width of FeII lines is 25% slower. Four days later, on $\Delta t = +6.5$ the emission line spectrum was getting much stronger (cf. the increase in equivalent width of Hα and FeII lines in Figs. 1 and 4), and the *FeII*-classification even clearer. Auroral [NII] 5755 Å and [OI] 5577 Å emission lines were becoming visible, as well as nebular [OI] 6300, 6364 Å. The intensity of the auroral lines was comparable to that of the nebular transition

lines, indicating high densities in the outermost neutral external regions of the ejecta where they formed.

On Δt = +18.4, ΔV = 2.6 mag, the [OI] lines grew in intensity more than the other lines, reminiscent of the *[OI] flash* (cf. PG57) seen in other novae at a similar evolution stage. The same happened to the [NII] lines and the NII+OII+NIII blend at 4640 Å on Δt = +36.4, ΔV = 3.3 mag when FeII weakened and HeI turned into weak emission, corresponding to the *[NII] flash* and *4640-phase* observed in many novae at ΔV = 3.0/3.5 mag (cf. PG57).

The reduced intensity of auroral with respect to nebular [OI] transitions in May indicates a decline in electronic density in the outer ejecta, as expected by the ongoing expansion and persistently low ionization stage.

5.3.3. OI lines

Emission lines from neutral oxygen offer several interesting applications for novae, some of which have been discussed by Strittmatter et al. (1977), Williams (1994), Bhatia & Kastner (1995), Kastner & Bhatia (1995), and Osterbrock (1989). Formalism and atomic constants in the present section were adopted from these sources.

The [OI] 5577, 6300, 6364 Å lines are among the first forbidden lines to appear in nova spectra thanks to their high critical densities. They persist even when [OIII] dominates the emission spectrum and high ionization lines appear (see for example the simultaneous presence of [FeVII] and [OI] lines in the spectra of Fig. 14). In the simplified case of spherically symmetric, homogeneous ejecta, created by a steady wind and photoionized by a central source, the [OI] lines trace ionization-bounded conditions and are expected to form in the external, neutral regions. The ratio of the 6300, 6364 Å nebular transitions under optically thin conditions is 3:1 from their transition probabilities, and it scales with optical depth τ (in the 6300 Å line) as

$$\frac{F_{6300}}{F_{6364}} = \frac{1 - \mathrm{e}^{-\tau}}{1 - \mathrm{e}^{-\tau/3}} \cdot \qquad (4)$$

At typical oxygen abundance, ejected mass and outflow velocity for a nova, [OI] 6300 Å should turn optically thin within the first few days after maximum brightness. Williams (1994) noted how the 6300/6364 Å flux ratio in novae is almost always lower than 3:1, indicating persistently optically thick conditions in the lines. He proposed that optically thick [OI] lines in novae come from small, very dense, neutral globules embedded in ambient, ionized ejecta and that the globules are internally powered by the decay of unstable isotopes produced by initial nuclear reactions (e.g. Hernanz 2005, and reference therein, for a discussion of unstable nuclides).

Figure 1 illustrates the evolution of 6300/6364 Å flux ratio over the whole outburst of NCyg06. The lines first appeared on the April 12 spectrum, ~10 days after the outburst onset, with a 2.2:1 ratio, and then initially evolved toward the 3:1 optically thin value. However, by late May 2006, when the decline of the nova slowed, the evolution of the 6300/6364 Å flux ratio reversed its course and progressively decreased, reaching the minimum value 1.1:1 by the time of second maximum. Such a low value requires $\tau \approx 7$. As soon as the nova entered the transition phase immediately following the second maximum, with the ionization spreading throughout the ejecta, the 6300/6364 Å ratio rapidly converged to the 3:1 value expected for optically thin conditions. The 6300 Å integrated line flux, on the other hand, displayed only a modest decline during the transition. Such a decline was confined to the phase when optically thin dust condensed (cf. Sect. 7 below), and afterwards the 6300 Å line progressively and rapidly regained the flux level it had reached *before* the transition phase.

The [OI] lines provide an estimate of the mass in the neutral region of the ejecta. Table 6 reports the results for some distinct epochs in the evolution of NCyg06, where Eq. (4) is used to derive the optical depth from the 6300/6364 Å flux ratio. The high-density conditions in the neutral regions make the auroral 5577 Å line easily detectable and therefore usable with the nebular 6300 Å line to estimate the electron temperature. How the latter correlates with the (reddening corrected) 5577/6300 Å flux ratio for a wide range of 6300 Å optical line depths is shown in Fig. 7. The proportionality between the integrated flux in the 6300 Å line and the amount of neutral oxygen in the ejecta as a function of optical depth and electron temperature is highlighted in Fig. 8 for the 7.2 kpc distance and E_{B-V} = 0.56 reddening derived earlier for NCyg06. The high density condition ruling the region of formation of OI lines is highlighted by the OI F_{8446}/F_{6300} emission line ratio. Its reddening-corrected value was 16.5 on Δt = 18.4 and Δt = 21.5. Comparing with the computation by Kastner & Bhatia (1995), it suggests a density $\geq 10^{10}$ cm^{-3}. The ratio lowered to 0.4, 2.8, 0.4, and 0.2 on Δt = 186, 253, 340, and 527, respectively, indicating a density $\geq 10^{8}$ cm^{-3}.

The data in Table 6 suggest that, at the beginning of the nova evolution, the neutral oxygen was present predominantly in the diffuse ejecta, while at the later stages it only survived in isolated, dense, and neutral globules. The mass of these globules accounts for ~1/12 of the total mass of the ejecta. This rough proportion can be derived by comparing the mass at first [OI] detection (Δt = 6.5 days), when nova ejecta were predominantly neutral, with the mass at advanced decline (Δt > 260 days) when the nova ejecta were essentially completely ionized (density bounded).

It will be shown in Sect. 11 that the ejecta of NCyg06 are oxygen enhanced (an O/H ratio ~32× larger than in the Sun). On Δt = 6.5 days, all oxygen in the NCyg06 ejecta was neutral, and therefore the mass derived for neutral oxygen corresponds to the total mass of oxygen in the ejecta ($M_{\rm O} = M_{\rm OI}$). Noting that the oxygen mass fraction derived in Table 9 from nebular analysis is 0.163 and that dust had not yet formed during early decline, the total mass of the ejecta can be estimated as

$$M_{\rm ejecta} = \frac{M_{\rm O}}{0.163} \approx 5 \times 10^{-4}\ M_{\odot} \qquad (5)$$

where $M_{\rm OI} = 8.1 \times 10^{-5}\ M_{\odot}$ is taken from Table 6. An independent estimate for $M_{\rm ejecta}$ will be obtained in Sect. 11 from analysis of the emission line spectrum in the nebular phase.

It is also noteworthy in Table 6 that the amount of neutral oxygen parallels the photometric evolution. In fact, in Sect. 5.1 we discussed how by June 1, 2006 the nova was departing from a pure exponential decline (to progressively slow its decline and later rise to a second maximum). At the same time, the amount of neutral oxygen (and presumably of neutral ejecta) was increasing, as if the ionization boundary was retracting (in a mass sense) through the ejecta.

The intensity of the OI 8446 Å emission line under normal recombination, optically thin conditions should be 3/5 of the OI 7774 line. The reddening-corrected flux ratio observed in NCyg06 is F_{8446}/F_{7774} = 7.7 on Δt = 18.4 (decline from

Table 6. The optical depth, electron temperature and mass of neutral oxygen in NCyg06 from the [OI] 5577, 6300 and 6364 Å emission lines. The listed epochs are those of the spectra showing the 5577 Å line in emission.

Δt (days)	$\frac{F_{6300}}{F_{6364}}$	τ_{6300}	$\frac{F_{6300}}{F_{5577}}$	$T_{\rm elec}$ (°K)	F_{6300}	$M_{\rm OI}$ ($M_\odot$)
6.5	1.304	4.23	2.133	4316	1.2e-11	8.1e-05
18.4	2.290	0.90	1.189	5927	2.3e-11	1.3e-05
21.5	2.479	0.61	1.330	5948	2.2e-11	1.0e-05
36.4	2.474	0.62	3.498	4859	1.4e-11	1.7e-05
50.3	2.417	0.70	4.336	4640	1.2e-11	1.7e-05
56.5	2.288	0.90	5.857	4338	1.5e-11	3.5e-05
78.3	2.190	1.07	10.844	3888	1.0e-11	4.5e-05
79.5	2.359	0.79	11.503	3924	1.2e-11	5.0e-05
96.3	2.283	0.91	10.412	3952	1.0e-11	3.9e-05
270.1	2.548	0.52	4.764	4629	4.4e-12	6.1e-06
282.2	2.553	0.51	4.243	4731	4.9e-12	6.1e-06
290.2	2.570	0.49	4.108	4768	7.4e-12	8.8e-06
339.6	2.796	0.22	6.138	4537	5.0e-12	6.7e-06

Δt: time since V brightness (April 5.6, 2006)
τ_{6300}: optical depth in the 6300 Å line
$T_{\rm elec}$: electronic temperature
$M_{\rm OI}$: mass of neutral oxygen
The flux ratios (F_{6300}/F_{6364} and F_{6300}/F_{5577}) and the F_{6300} integrated line flux (in erg cm^{-2} sec^{-1}) are corrected for the E_{B-V}=0.56 reddening affecting NCyg06

first maximum), 21.5 on Δt = 290 (decline from second maximum), and 12.5 on Δt = 340 (nebular condition during the advanced stages of the final decline). The inversion in intensity between the two OI lines is usually associated with fluorescence pumped by absorption of hydrogen Lyman-β photons, as first pointed out by Bowen (1947). For the Lyman-β fluorescence to be effective, the optical depth in Hα should be large, presumably owing to the population of the n = 2 level by trapped Lyman-α photons. The $F_{8446}/F_{\rm H\alpha}$ under optically thin, low ionization conditions and typical nova chemical abundances is quite low, $\sim 10^{-3}$ (Strittmatter et al. 1977). The evolution of the $F_{8446}/F_{\rm H\alpha}$ flux ratio for NCyg06 is presented in Fig. 1. It reached a much higher ~0.5 value during early evolution (on Δt = 18.4 and 21.5). It indicates a very large optical depth in Hα, in agreement with the ejecta still being predominantly neutral and very dense at that time. At later times the picture was more confused due to the clumpiness of OI-emitting regions described earlier and the growing [NII] contribution to the Hα observed flux. Nevertheless, even at advanced evolutionary stages, the $F_{8446}/F_{\rm H\alpha}$ did not decline below 0.05, indicating persistent (even if reduced) optically thick conditions in Halpha. This agrees with the evidence from the F_{8446}/F_{7774} ratio that Lyman-β fluorescence has remained effective throughout all NCyg06 evolutionary stages.

6. The plateau phase

When NCyg06 left the exponential decline of Eq. (1) around June 1, it had magnitudes and colors of V = 11.83, $B-V$ = +0.28, $V-R_{\rm C}$ = +1.44, $R_{\rm C}-I_{\rm C}$ = +0.20 and $V-I_{\rm C}$ = +1.64. A minimum brightness was reached on July 15 at V = 12.15, $B-V$ = +0.15, $V-R_{\rm C}$ = +1.28, $R_{\rm C}-I_{\rm C}$ = −0.01 and $V-I_{\rm C}$ = +1.27. During the following rise in brightness, the same V-band brightness as for June 1 was regained 111 days later on September 20, when it was V = 11.83, $B-V$ = +0.16, $V-R_{\rm C}$ = +0.91, $R_{\rm C}-I_{\rm C}$ = +0.07 and $V-I_{\rm C}$ = +0.99.

The significantly bluer colors on September 20 compared to June 1 indicate that the nova had appreciably evolved. This is clear from the evolution of the spectrum (illustrated in Fig. 9) during this plateau period. Progressively, FeII emission disappeared, while NII/Hβ and NIII+Hδ/Hγ increased, and [NII] decreased with respect to NII and increased compared to [OI]. However, the most interesting feature of this plateau period is the re-emergence of the Orion absorption system. The Orion absorptions were last seen on the May 11 spectrum and marginally still visible on June 1. On the August 21 and September 26 spectra of Fig. 9, the most notable Orion absorption lines are those of HeI 3889 Å (−2140 km s^{-1} radial velocity), 4471 (−2065 km s^{-1}), 5876 (−2260 km s^{-1}), OII 4321 (−2125 km s^{-1}), NII 4601 (−2100 km s^{-1}), 4788 (−2150 km s^{-1}), 5672 (−2100 km s^{-1}). Particularly interesting is the re-emergence of NIII 4097-4103 (−1950 km s^{-1}) on the September 26 spectrum (compare the Hδ blue wing with that of the June 1 spectrum on Fig. 9). The average velocity of the Orion absorptions on September 26 was −2100 km s^{-1}, significantly higher than on June 1 when the Orion spectrum was last seen (cf. Table 5). The acceleration seen in the Orion absorptions had the reverse sign for NIII 4097−4103: −2200 on June 1 and −1950 km s^{-1} on September 26.

During this plateau period, we obtained high-resolution Hα profiles on June 1 and 24, July 18 and 29, August 31 and September 26. The Hα profles from June 1 to August 31 are all the same and very similar to that of June 24 shown in Fig. 12, which is characterized by a multi-peaked top and by 1340 km s^{-1} full width at half intensity. On the other hand, the September 26 profile is characterized by the emergence of a hazy, broad and featureless pedestal whose full width at zero intensity approaches 6000 km s^{-1}, while the width at half intensity is ~4200 km s^{-1} (matching the ~−2100 km s^{-1} expansion velocity of the Orion absorption lines). This pedestal grew conspicuously in relative intensity by the time of secondary maximum (cf Fig. 12). It is worth noticing that the decline of the Orion absorptions in novae is usually accompanied by the emergence in emission line profiles of hazy and broad components, even if Balmer lines do not always display them.

7. The second maximum

The second maximum was reached by NCyg06 at V = 9.95 around HJD 2 454 071.4 (December 1, 2006) at Δt = +239.0 and ΔV = 1.95, with colors $U-B$ = −0.29, $B-V$ = +0.28, $V-R_{\rm C}$ = +0.68, $R_{\rm C}-I_{\rm C}$ = +0.28, $V-I_{\rm C}$ = +0.98. The emission lines at that time had a minimal impact on the overall energy distribution, and the intrinsic $(B-V)_\circ$ = −0.28 corresponds to that of a B0 giant, compared to an F0 giant at first maximum. Compared to the first maximum, the colors at the second maximum were bluer by the following amounts: $\Delta(B-V) \approx -0.60$, $\Delta(V-R_{\rm C}) \approx -0.42$, $\Delta(R_{\rm C}-I_{\rm C}) \approx -0.20$ and $\Delta(V-I_{\rm C}) \approx -0.52$ (colors at t = 0 are extrapolated by parabolic fitting to the early decline data in Table 1 and Fig. 1). The time required to rise the last magnitude in the V band was 22 days, to decline the first two magnitudes was 9.6 days, and to decline the first three magnitudes was 11.9 days. The brightness and color evolution around the second maximum is highlighted in Fig. 10.

The overall spectroscopic aspect of NCyg06 at the second maximum was appreciably different than at the first one, as seen when comparing the spectral evolution in Fig. 5 with Fig. 11). In addition to the Balmer series, only low-excitation absorption

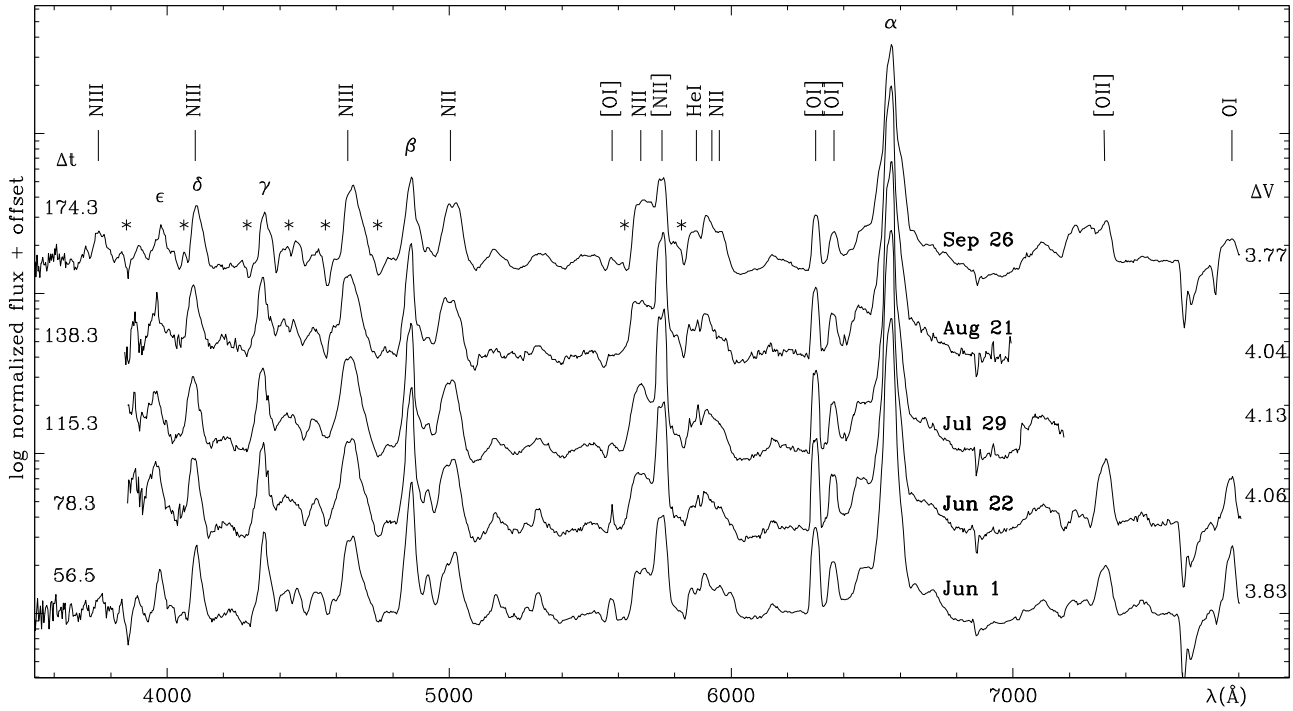

Fig. 9. Spectroscopic evolution of Nova Cyg 2006 during the plateau phase in June−September 2006 (see Fig. 5 for plotting details). The asterisks mark the positions of the principal Orion absorption lines on the September 26 spectrum (see Sect. 6 for the line list).

lines (mainly CaII, NaI, FeII) were seen at the first maximum, in agreement with the F0 underlying spectral energy distribution. At second maximum, the underlying continuum was much hotter and the excitation of the absorption spectrum correspondingly much higher. The strongest, non-Balmer absorption lines were: CII 6789, 6746, 5143; NII 6482, 5678, 5667, 5045, 5007, 4791, 4602; NIII 4639, 4513, 4100; OII 4495, 4468, 4416, 4318, 4070 and HeI 6678, 5876, 4471, 3889. Their mean radial velocity was −2190 km s^{-1} for CII, −2135 km s^{-1} for NII, −2070 km s^{-1} for OII, and −2170 km s^{-1} for HeI. The absorption spectrum at second maximum represents the re-emergence of the Orion system that disappeared during the plateau phase.

Quite interesting are the absorption components seen in Hα during the second maximum. The spectrum for November 5, 2006 in Fig. 12 is representative of them. The underlying emission is obviously much more structured compared to the simple, symmetric one seen during first maximum (cf. Fig. 6), and therefore unambiguous identification of weaker absorptions is severely affected. Nevertheless, at least two strong absorptions are safely identified: one centered at −905 km s^{-1} (*VHM* = 145 km s^{-1}, *e.w.* = 1.90 Å, integrated flux = 8.4×10^{-13} erg cm^{-2} s^{-1}), the other at −2215 km s^{-1} (*VHM* = 355 km s^{-1}, *e.w.* = 7.67 Å, integrated flux = 2.0 × 10^{-12} erg cm^{-2} s^{-1}). They could be tentatively identified with the re-emergence of *principal* and *diffuse-enhanced* absorption systems seen during the decline from the first maximum (cf. Table 4). On November 22, the faster of the two components had grown to an integrated flux of 3.5 × 10^{-13} erg cm^{-2} s^{-1} and an equivalent width 9.8 Å.

Similar to what has just been described for the absorption spectrum, the emission spectrum at second maximum was quite different from that at first maximum, reflecting the much higher temperature of the underlying continuum. At second maximum, FeII emission lines were not seen and were replaced by NII, NIII, OII, [OI], and HeI. [NII] 5755 disappeared, and the F_{6300}/F_{6364} ratio approached 1.1:1 (cf. Fig. 1 and Sect. 5.3.3). Overall, the strong decrease in equivalent width of the emission lines at secondary maximum (cf. Hα behavior in Fig. 1) essentially stemmed from the increase in the underlying continuum. The evolution of integrated flux of emission lines went unaffected through the development of second maximum, as the evolution of [OI] and Hα in Fig. 1 illustrates.

8. Final decline

Soon after the second maximum was reached on December 1, NCyg06 entered the final decline that is continuing up to now. During this phase, NCyg06 resumed the normal spectroscopic evolution of a nova that was interrupted by the plateau phase and rose to secondary maximum. The decline is characterized by a sharp change in the slope of the lightcurve occurring around December 12, as illustrated by both Figs. 1 and 10. That date also marks the transition of NCyg06 from stellar to nebular spectral type.

8.1. Decline prior to December 12

Between the second maximum and December 12, the nova became fainter by $\Delta V = 2.8$ mag in 11 days, with $t_2^V = 9.6 \pm 0.2$ and $t_3^V = 11.9 \pm 0.3$ days. The slope of the declines from the first and second maxima are quite different, as the respective t_2/t_3 suggest and a comparison of Figs. 4 and 10 supports. The rate of decline from first maximum was slowing with time, that from second one was increasing with time. The $B - V$ color initially turned bluer as the stellar continuum turned hotter, but this was short-lived and by December 8 it reversed the trend. By December 13 it had resumed the smooth course it has been displaying since the earliest outburst phases (cf. Fig. 10). The $V - R_C$ color increased almost exponentially from December 7 to 12, as a result of the rapidly growing relative contribution of Hα to R_C-band

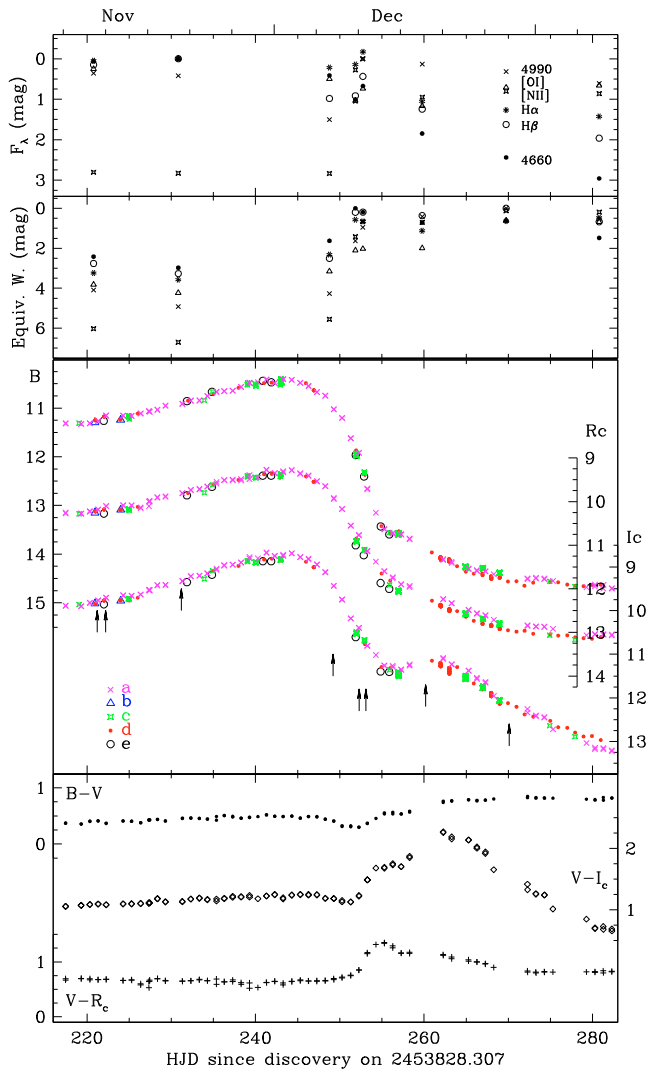

Fig. 10. *Middle panel*: photometric evolution of Nova Cyg 2006 around second maximum. *B*-band lightcurve is *at the top*, R_C *center*, I_C *bottom*. For telescope identification letters see Sect. 2.1. *Bottom panel*: color evolution as recorded with telescope *a*. *Upper panels*: evolution of integrated flux and equivalent width of selected emission lines, expressed in magnitudes with respect to highest value. The *4660* blend is initially dominated by NIII, than HeII become a relevant contributor. The *4990* blend is initially due to NII, then [OIII] becomes the dominant contributor.

(cf. Hα equivalent width evolution in Fig. 1). The extra flux in the I_C-band, clearly influencing $R_C - I_C$ and $V - I_C$, will be discussed in Sect. 9 below.

The strong multiple absorptions seen in the Balmer lines and the Orion absorption system, so prominent at the time of second maximum, quickly vanished after the maximum. The only absorption lines still present in the December 10 spectrum are NII 4601, NIII 4097-4103, OIII 5592 Å, and a weak, residual -1750 km s^{-1} absorption component in Hα. They too had vanished by December 12. The emission line spectrum during decline from second maximum changed much less than during decline from primary maximum. The ionization/excitation increased only modestly, while there was a strong increase in equivalent width of the emission lines. The major change was seen in the optical depth of [OI] that soon started to decline from $\tau_{6300} \approx 7$ at maximum, to $\tau_{6300} \approx 0.15$ on December 12.

8.2. Decline after December 12

Around December 12 the rapid decline of NCyg06 from the second maximum suddenly slowed down, settling to a $\langle \Delta B \rangle = 0.0088$ mag day^{-1} straight linear slope over the range $+300 \leq \Delta t \leq +460$. This transition in the photometric evolution corresponds to the transition from stellar to nebular spectral types. In fact, the spectrum for December 10 in Fig. 11 is still dominated by the continuum emission with a modest contribution from emission lines. Three days later (cf. December 13 spectrum in Fig. 11), the spectrum had already turned into the nebular type, with a huge increase in the equivalent width of emission lines and weakening of the underlying continuum. In particular, [OIII] 4363 was emerging on the red wing of the Hγ profile, [OIII] 4959, 5007 were already key contributors to the strong emission blend with NII centered at 4990 Å, [NII] 5755 was already stronger than Hβ, and HeII 4686 was becoming detectable superimposed over the huge NIII emission at 4640 Å. During the first weeks of the nebular state, nebular lines appeared double-peaked with a peak-to-peak velocity separation of 595 km s^{-1} for [OI] 6364, 815 km s^{-1} for [NII] 5750, and 950 km s^{-1} for [OIII] 5007 Å.

With the transition from stellar to nebular type, the emission from the rapidly growing fraction of ionized ejecta compensated for the rapid photometric decline associated with the retracting pseudo-photosphere, which was increasing in temperature and therefore was shifting the peak of its emissivity to shorter and shorter UV wavelengths. The reprocessing into $UBVR_CI_C$ bands and longer wavelengths of ultraviolet flux absorbed by the ionized ejecta resulted in the leisurely $\langle \Delta B \rangle = 0.0088$ mag day^{-1} decline rate and in the protracted visibility of the nova for such a long period. Without reprocessing ejecta, the central source would have become unobservable in the optical by January 2007.

8.3. The fast and tenuous wind of mid 2007

As illustrated by the spectra in Fig. 14, in July–September 2007 the emission lines grew in width. The *FWHM* of [OI] lines increased from 1325 km s^{-1} on March 11 spectra, to 1870 km s^{-1} on July 20, and 1890 km s^{-1} on September 19, and [NII] lines from 1570 km s^{-1} to 2070 and 2135 km s^{-1}, respectively. This trend is illustrated in Fig. 1, which also shows how the photometric decline almost stopped during the same period, with an extra ~0.6 mag flux in the *B* and *V* bands with respect to extrapolated earlier lightcurves. We interpret these events as due to the emergence of a fast, tenuous wind from the central star. Its effects are equally evident in the evolution of the blended Hα+[NII] profile in Fig. 12.

9. Dust formation

Infrared photometry of NCyg06 is available from the literature for only three dates: April 30, June 14, and December 12, 2006 (Russell et al. 2006; Mazuk et al. 2006; Lynch et al. 2006). These IR magnitudes were combined with our simultaneous $UBVR_CI_C$ from Table 1 to construct the spectral energy distributions shown in Fig. 13, where the interpolating blackbodies have been reddened to the $E_{B-V} = 0.56$ affecting NCyg06. On April 30 and June 14, the $UBVR_CI_CJHK$ spectral energy distribution can be ascribed entirely to emission from the pseudo-photosphere with no contribution from warm dust, while on December 12 ($\Delta t = +251^d$) thermal emission from dust is quite apparent.

The dust detected on December 12 was optically thin. The energy re-emitted by dust in the infrared is energy absorbed from

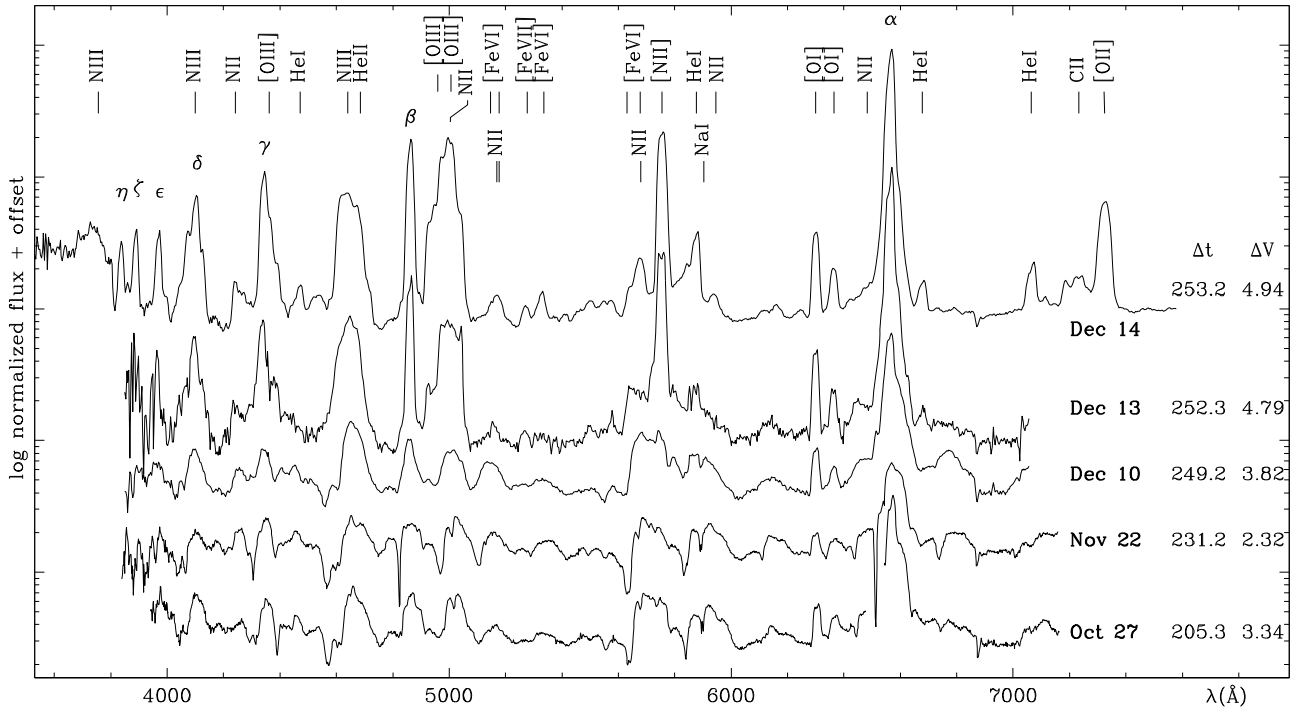

Fig. 11. Spectroscopic evolution of Nova Cyg 2006 during second maximum in autumn 2006 (see Fig. 5 for plotting details).

energy radiated by the nova, and therefore the dust optical depth is $\tau = L_{\rm IR}/L$. L is difficult to estimate directly at the time of dust condensation because most of it is radiated in the ultraviolet as indicated by the nebular and high ionization condition of the ejecta and illustrated by the spectral energy distribution of Fig. 13. However, theoretical models argue for a prolonged *plateau* period of constant luminosity experienced by novae following optical maximum (Prialnik 1990, and references therein), which is confirmed by multi-wavelength observations of well studied novae (Gallagher 1977; Gallagher & Starrfield 1978; Gehrz et al. 1998). It can therefore be written that

$$\tau_{\rm dust} = \frac{L_{\rm IR}}{L_{\rm plateau}} \cdot \qquad (6)$$

In Sect. 11 below, we show from photo-ionization modeling that on January 20, 2007 ($\Delta t = +290$) the bolometric luminosity of NCyg06 was $M_{\rm bol} = -6.45$ corresponding to $L_{\rm bol} = 1.3 \times 10^{38}$ erg s^{-1}. We assume this was valid for December 12, 2006 as well. The luminosity radiated by the 1550 K blackbody fitting the December 12 dust emission over the L, M, and N-band photometric points of Fig. 13 is $L_{\rm max} = 2.6 \times 10^{37}$ erg s^{-1}. The optical depth of the dust for December 12 is therefore $\tau_{\rm dust} \sim 0.2$, indicating optically thin conditions.

The infrared data available for NCyg06 do not enable a derivation of physical properties of the dust. However, for sake of discussion, we assume that the dust grains condensed in NCyg06 followed the mean properties observed in other novae (Gehrz 1988; Mason et al. 1996; Evans et al. 1997; Gehrz et al. 1998), i.e. they were small carbon grains (radius $a \leq 1$ μm, density $\rho \sim 2.3$ gr cm^{-3}), for which the Planck mean emission cross section goes as $Q_{\rm e} = 0.01 a T_{\rm dust}^2$. Under these assumptions, the mass of the dust in NCyg06 on December 12 is

$$M_{\rm dust} = 1.17 \times 10^6 \rho T_{\rm dust}^{-6} \left(\frac{L_{\rm IR}}{L_\odot} \right) = 1.3 \times 10^{-9}\ M_\odot \qquad (7)$$

which is quite small. Comparing with the amount of gas in the ejecta estimated below in Eq. (9), the gas-to-dust ratio in the ejecta on that date is $\left(\frac{M_{\rm gas}}{M_{\rm dust}}\right) \approx 3 \times 10^5$. A similarly high value of the gas-to-dust ratio has been previously observed in Nova Vul 1984 N.2, which, like NCyg06, displayed a large oxygen overabundance ([O/H] = +1.6, Gehrz et al. 1998). It should also be noted that dust did not appear to form in some other novae, adequately observed in the infrared.

As a first guess, it may seem that the hard radiation field from the central star, responsible for the ionization of the ejecta, should suppress dust grain formation (e.g. Gallagher 1997). Actually, observations of well-studied novae indicate that dust condenses when the ejecta become optically thin in the near ultraviolet and the nova spectrum shifts from stellar to nebular type. Shore & Gehrz (2004) proposed that ionization may be a promoting agent of dust condensation via ionization-mediated kinematic agglomeration of atoms onto molecules and small grains through induced dipole interactions. It is interesting to note that dust was detected in NCyg06 on December 12, right when the transition was taking place. When comparing the December 10 and December 13 spectra in Fig. 11, the huge increase in both the amount and excitation degree of nebular emission is outstanding. Description of the infrared observations by Rayner et al. (2006) indicates that dust emission was absent on November 30 (when the nova was peaking at second maximum), and was still present on December 20 when the transition to a nebular spectrum was completed ([OIII] 4949 and [NII] 5750 Å appreciably stronger than Hβ). They estimated a black-body temperature of 1410 K beyond 2 μm. Once corrected for the $E_{B-V} = 0.56$ reddening affecting the nova, their estimate is in fair agreement with our derived 1550 K for December 12 data.

Such a temperature is unusually high for dust grains in novae (cf. Gehrz 2002). However, it has to be noted that on December 12 the dust had just begun to form in NCyg06 (a matter of a few days or even hours), it had a quite thin optical depth and it was quite low in mass. These are conditions away from the average ones applying to the novae for which dust properties

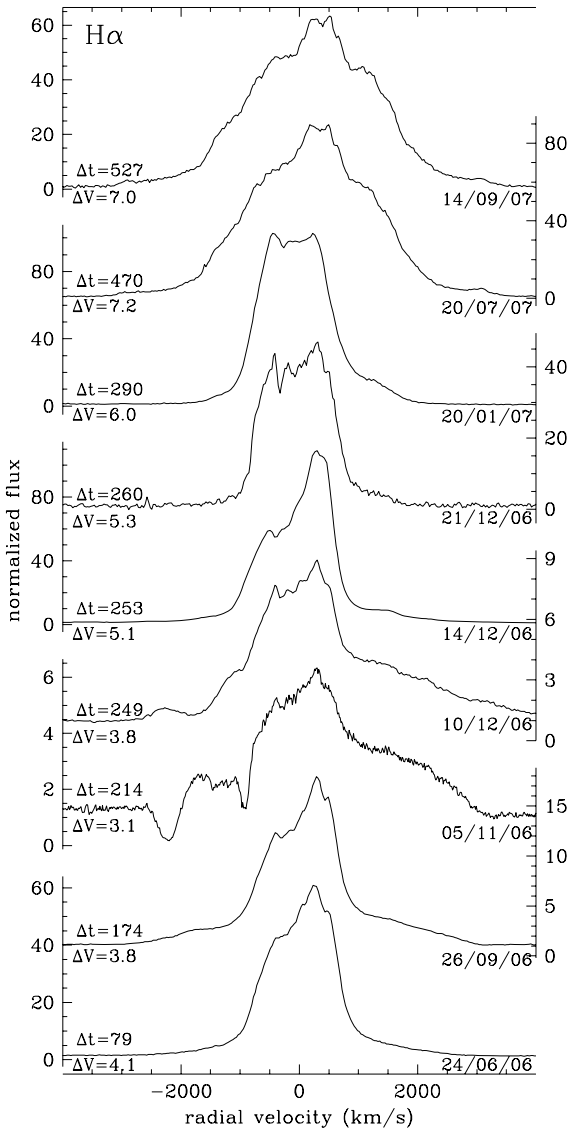

Fig. 12. Evolution of Hα profile during the plateau phase, the second maximum and the advanced decline. Δt and ΔV are days and magnitudes from maximum.

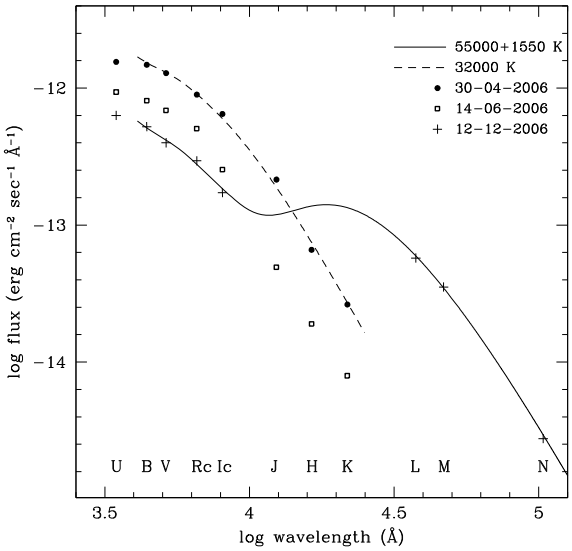

Fig. 13. The optical and infrared spectral energy distribution of Nova Cyg 2006 showing the presence of optically thin dust emission on December 2006. Optical data are from Table 1, and infrared data from Russell et al. (2006), Mazuk et al. (2006), and Lynch et al. (2006). The curves are fits with black bodies at the indicated temperatures and reddened by $E_{B-V} = 0.56$ following a $R_V = 3.1$ standard law.

have been studied in detail. We do not discuss the dust temperature in NCyg06 further, since we lack the necessary infrared data. In particular, contribution by emission silicate features at 10 μm and hydrocarbon features at 3.3, 3.4, and 11.3 μm have been observed in some novae superimposed onto the carbon dust continuum during the optically thin phase (for ex. in V705 Cas by Gehrz et al. 1995; or V842 Cen by Gehrz et al. 1990). The presence of these (strong) emission features may alter the slope of the spectral energy distribution and consequently spoil the significance of temperature estimates from black-body fitting to broad-band photometric measurements.

An intriguing feature of NCyg06 is the I_C band excess it displayed during the second half of December (see Fig. 10), soon after the dust detection on December 12. Following the second maximum, all bands declined steeply and in a similar fashion, with a marked slope change around December 12 when the transition from stellar to nebular spectrum took place and the ionization spread widely through the ejecta. From that date, all bands declined linearly with time, except I_C, which displayed a pronounced extra-emission of $\Delta I_C \approx 1$ mag amplitude peaking around December 21 (see Fig. 10). During this time interval, we did not obtain spectra covering the I_C wavelength range. The closest spectra were taken on December 12, when the transition to nebular spectrum was already rapidly proceeding, and it shows only a modest OI 8446 Å emission line and a weak Paschen continuum in emission, neither of which are able to account for a sizable fraction of the I_C flux. We are therefore inclined to exclude a flaring of emission lines selectively concentrated over its wavelength range as the cause of extra emission in the I_C band during the second half of December. This is also supported by the evolution of the $V - R_C$ color illustrated in Fig. 10, which was dominated by the huge increase in the Hα equivalent width (cf. Fig. 1) induced by the nova transition to the nebular stage (on the December 21 spectra, at the time of I_C band bump maximum, Hα was accounting for 0.63 mag of the whole flux in the R_C band). The $V - R_C$ color evolution is smooth and linear throughout the I_C bump development.

The only feasible source of extra-emission that could have been responsible for the I_C December bump seems to be the dust. For dust emission to have leaked into the I_C band, it must have condensed into larger quantities and/or peaked to hotter temperatures than on December 12. A choice between the two alternatives could be possible only with the support of (missing) infrared data covering the second half of December.

10. Comparison with V1493 Nova Aql 1999a

The lightcurve of NCyg06 has been highly peculiar, but not completely unprecedented. A close match is represented by Nova Aql 1999 N.1 (=V1493 Aql), and Fig. 15 compares the V-band lightcurves of the two novae. The similarity is striking, with V1493 Aql requiring 5.0× less time to go from primary to secondary maximum, even if its $t_2 \approx 7$ and $t_3 \approx 23$ days (Venturini et al. 2004) are not that different from $t_2 = 10.4$ and $t_3 = 24$ of NCyg06. Both novae seem to have orbital periods above the period gaps of cataclysmic variables, 5.0 h

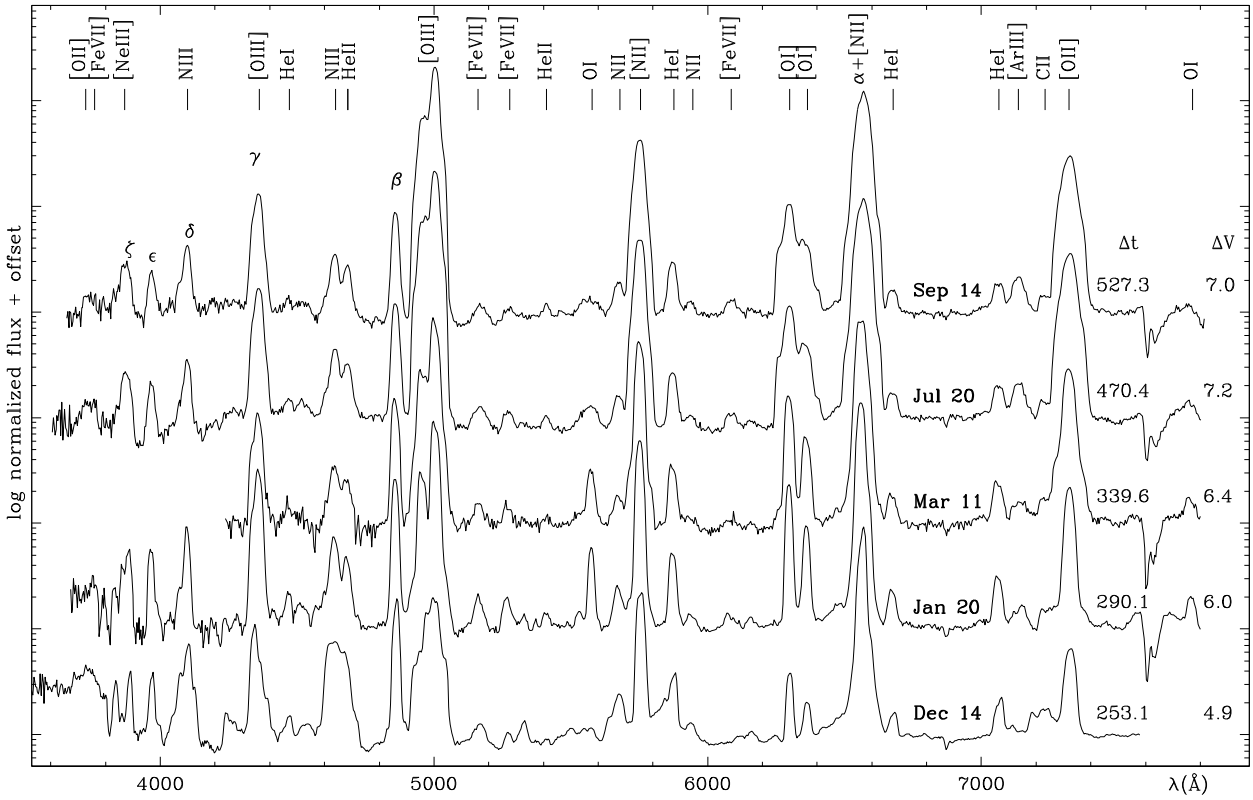

Fig. 14. Spectroscopic evolution of Nova Cyg 2006 during the advanced decline from December 2006 to September 2007 (see Fig. 5, for plotting details).

for NCyg06 (Goranskij et al. 2006) and 3.7 h for V1493 Aql (Dobrotka et al. 2006). Both novae belong to the FeII class and shared similar expansion velocities at first (*FWHM* = 1700 km s^{-1} for V1493 Aql, Arkhipova et al. 2002) and second maximum (*FWHM* = 2000 km s^{-1} for V1493 Aql, Venturini et al. 2004). The spectral evolution of V1493 Aql has been poorly monitored. However, what is recorded suggests a path parallel to that of NCyg06: (*a*) low ionization conditions at both primary (only Balmer and FeII lines in emission in optical spectra, Tomov et al. 1999) and secondary maxima (only Paschen, Bracket, OI and NI lines in emission with marginal HeI in IR spectra, Venturini et al. 2004), (*b*) slight increase in ionization between the two maxima with appearance of OII, [OIII], NII and [NII] emission lines and disappearance of FeII (Arkhipova et al. 2002), (*c*) spectra obtained during the advanced decline characterized by nebular conditions, with [OIII], [NII] and NIII among the strongest emission lines (Arkhipova et al. 2002).

The only possible major difference could be in the color evolution. Bonifacio et al. (2000) assembled heterogeneous $B-V$ measurements published in several IAUC with some of their own, and concluded that V1493 Aql was hotter at maximum light ($B-V < 0.4$) than at secondary peak ($B-V \sim 1.2$) or plateau phase ($B-V \sim 0.9$), with a bluer color during advanced decline ($B-V \sim 0.7$). Unfortunately, the intrinsic variability of the comparison stars chosen by Bonifacio et al. to reduce their own measurements and the wild heterogeneity of the measurements collected from the literature does not call for any high confidence in the results. The reported color evolution could have been strongly affected by contamination to the *V*-band by the extremely strong Hα emission displayed by V1493 Aql. Another word of caution about the Bonifacio et al. (2000) results is the excessively blue color they report for t_2, $B-V = 0.32$. After correcting it for the $E_{B-V} = 0.6$ derived by

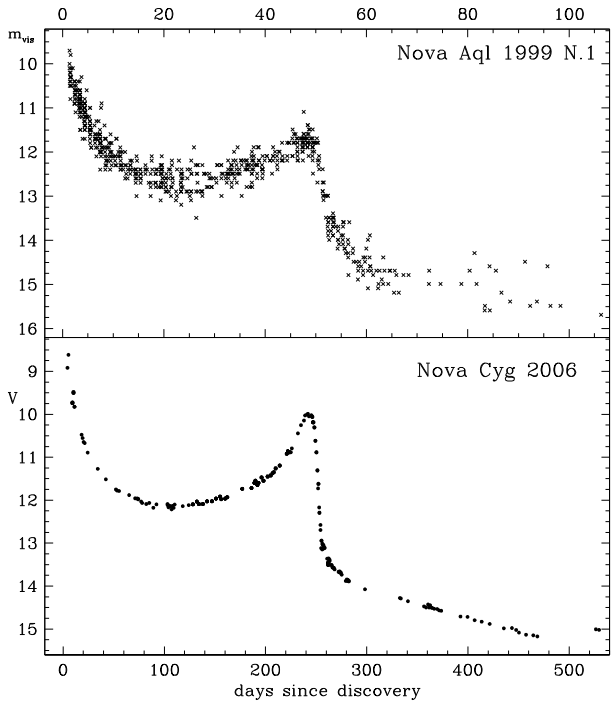

Fig. 15. Comparison of Nova Cyg 2006 *V*-band lightcurve with the m_{vis} lightcurve of Nova Aql 1999 N.1 (AAVSO visual estimates). The ordinate scale is the same in both panels. The time scale of Nova Aql 1999 N.1 abscissas is 5.0× faster that that of Nova Cyg 2006.

Venturini et al. (2004), the intrinsic color would be $(B-V)_\circ = -0.3$, equal to that of the hottest known stars ($(B-V)_\circ = -0.32$ for O5 stars, Fitzgerald 1970), which contrasts with the cool temperature of the pseudo-photosphere required by the very low ionization condition of the emission line spectrum. The discrepancy would be even greater if the $E_{B-V} = 1.5$ reddening estimated by Arkhipova et al. (2002) would be adopted instead. The $(B-V)_\circ = -0.3$ color at t_2 also sharply contrasts with the average $(B-V)_\circ = -0.02$ derived by van den Bergh & Younger (1987) and also perfectly matched by NCyg06 (cf. Sect. 4 above). In conclusion, we are highly suspicious of the odd color evolution reported by Bonifacio et al. (2000) for V1493 Aql, and consider it worth further investigation.

11. Photo-ionization analysis

A photo-ionization analysis of NCyg06 spectrum for January 20, 2007 ($\Delta t = +290^d$) has been performed with the CLOUDY code, version c06 (Ferland et al. 1998). This is the spectrum (plotted in Fig. 14) during the nebular phase with the highest S/N and lower line blending, before the flaring of the line profile widths seen at later phases (cf. Fig. 12). A detailed modeling of all collected spectra is far beyond the scope of this paper, and will be considered elsewhere. Nevertheless, the results we obtained for the January 20, 2007 spectrum are confirmed by preliminary CLOUDY analysis of the other spectra, especially concerning chemical abundances.

We assumed spherically expanding ejecta with a gas density declining as $\rho(r) \propto r^{-2}$. We explored other density profiles ($\rho(r) \propto r^n$, with $n = 0, -1$, and -3), but obtained a poorer match with observations. We did not fix inner and outer radii for the ionized shell ($r_{\rm in}$ and $r_{\rm out}$), and treated them as free parameters along with the ratio of the filled to the vacuum volumes in the ejecta (ξ). Only the abundances of chemical elements with observed lines were allowed to change, and all others were kept fixed to their solar value. Table 7 lists the observed and computed fluxes for the emission lines used in the modeling, Table 8 summarizes the modeling results that are discussed below, and Table 9 provides the corresponding chemical mass fractions.

11.1. Internal and external radii

The shell of ionized gas at $\Delta t = +290^d$ is a thin one, extending from $r_{\rm in} = 149$ to $r_{\rm out} = 168$ AU. The inner radius is a density boundary (no interior matter). The outer one is an ionization boundary, defined by the distance at which the electronic temperature drops to negligible values (all ionizing photons are absorbed within $r_{\rm out}$, and only neutral material could exist outward). These radii correspond to expansion velocities of 890 and 1010 km s^{-1}. It is worth noticing that this is within the range of velocities displayed by the p_1 *principal* systems of the multi-component absorption spectrum, that it was the first to appear, the longest lived, and the one carrying the largest mass outflow, as Fig. 6 and Table 4 clearly illustrate. Therefore, the ejected material causing the p_1 *principal* absorption systems during early post-maximum decline appears to be the same, creating most of the emission line fluxes at $\Delta t = +290^d$ during the nebular phase.

11.2. Mass in the shell

The hydrogen mass fraction in the ionized shell is $X = 0.427$, and the ratio of the filled to vacuum volumes is $\xi = 0.12$.

Table 7. De-reddened emission line ratios relative to Hβ as observed on the Jan. 20, 2007 spectrum of Nova Cyg 2006 and as predicted by the CLOUDY model detailed in Table 8.

line	*obs*	*comp*
Hα + [NII] 6548-84	4.50	3.40
Hβ	1.00	1.00
Hγ + [OIII] 4363	1.96	3.27
Hδ	0.36	0.29
Hϵ		0.19
H8	0.20	0.13
5876 HeI	0.14	0.14
7065 HeI	0.06	0.08
4686 HeII	0.20	0.14
4679 NII	0.06	0.07
5755 [NII]	1.95	1.70
4640 NIII	0.38	
6300 [OI]		
7325 [OII]	0.70	0.57
4959 [OIII]	1.32	1.16
5007 [OIII]	4.30	3.40
3869 [NeIII]	0.10	0.12
4720 [NeIV]	0.005	0.0045
7135 [ArIII]	0.016	0.016
7236 [ArIV]	0.0013	0.0016
7006 [ArV]	0.0024	0.0023
6087 [FeVII]	0.007	0.007

Table 8. Parameters of the CLOUDY model best-fitting the de-reddened emission line ratio of Table 7. *From top to bottom*: temperature and radius of the central black-body source, inner and outer radii of the emitting shell, hydrogen density at inner and outer radii, electronic density at the inner and outer radii, ratio of the filled to vacuum volumes, element abundances relative to solar.

$\log T_{\rm BB}^{\rm eff}$ (K)	5.236
$\log R_{\rm BB}$ (cm)	10.14
$\log r_{\rm in}$ (cm)	15.35
$\log r_{\rm out}$ (cm)	15.40
$\log \rho_{\rm in}^H$ (cm^{-3})	7.781
$\log \rho_{\rm out}^H$ (cm^{-3})	7.874
$\log N_{\rm in}^e$ (cm^{-3})	8.00
$\log N_{\rm out}^e$ (cm^{-3})	5.00
ξ	0.12
H/H$_\odot$	0.80
He/He$_\odot$	0.87
N/N$_\odot$	316
O/O$_\odot$	26
Fe/Fe$_\odot$	1.0
Ar/Ar$_\odot$	1.0
Ne/Ne$_\odot$	1.0

Therefore, the total gas mass within the ionized shell at $\Delta t = +290^d$ is

$$M_{\rm shell} = \frac{\xi}{X} \int_{r_{\rm in}}^{r_{\rm out}} 4\pi r^2 \rho(r) {\rm d}r = 3 \times 10^{-4}\ M_\odot. \quad (8)$$

In Sect. 5.3.3 we estimated from the [OI] lines the amount of neutral gas in the ejecta during the early days of the decline from maximum when the ejecta were predominantly neutral, and found $M_{\rm ejected}^{\rm total} = 5 \times 10^{-4}\ M_\odot$ (Eq. (5)). The agreement of

Table 9. Mass-fraction abundances of measured elements in Nova Cyg 2006 and, for reference, in the Sun.

	mass-fractions	
	NCyg	*Sun*
X	0.427	0.704
Y	0.185	0.279
Z	0.388	0.017
N	0.219	0.001
O	0.163	0.008
Ne	0.0013	0.0017
Ar	0.00008	0.00011
Fe	0.00096	0.00126

the two estimates is quite reassuring, in particular if it is taken into account that the ionized shell at $\Delta t = +290^d$ is radiation-bounded and neutral material could exist outward. Therefore $M_{\rm shell} = 3 \times 10^{-4}\ M_\odot$ is a lower limit to the total amount (ionized + neutral) of gas existing at $\Delta t = +290^d$. For sake of discussion in the rest of the paper, we assume for the total amount of ejected material an averaged value between the two methods:

$$M^{\rm total}_{\rm ejected} = 4 \times 10^{-4}\ M_\odot. \quad (9)$$

11.3. Central star

The central ionizing source is found to have a radius $R = 0.198\ R_\odot$, a temperature $T_{\rm eff} = 172\,000$ K, and therefore a luminosity $3.08 \times 10^4\ L_\odot$, corresponding to $M_{\rm bol} = -6.45$ (assuming $M_{\rm bol} = 4.74$ for the Sun, Livingston 2000).

11.4. Mass of the white dwarf

At the time of the January 20, 2007 spectrum, NCyg06 was undergoing the luminosity plateau phase. It characterizes the observed and theoretical evolution of novae after the initial super-Eddington phase and before the switching-off of the nuclear reactions and consequent cooling track for the white dwarf (cf. Gehrz et al. 1998). During the luminosity plateau phase, the white dwarf burning residual hydrogen at the surface follows the Paczyński core-mass-luminosity relation $L_{\rm cnl} = 6 \times 10^4 (M_{\rm WD}/M_\odot - 0.522)\ L_\odot$. Inserting the above estimated luminosity, the mass of the white dwarf turns out to be

$$M_{\rm WD} = 1.03\ M_\odot. \quad (10)$$

The amount of material to be accreted on this white dwarf for the pressure to reach 10^{20} dyne and trigger a TNR event is $4 \times 10^{-4}\ M_\odot$ (cf. Starrfield 1989). In comparison with Eq. (9), the outburst therefore seems to have ejected most of material accreted by the white dwarf before the eruption set in.

11.5. Chemical abundances

The chemical abundances in the ionized shell are given in Table 8 (relative to solar) and Table 9 (as mass fractions). They clearly reflect the non-equilibrium CNO-cycle burning of hydrogen, with massive overabundance of oxygen and nitrogen, among the largest ever measured in novae. Carbon should be enhanced too, but there were no detectable carbon emission lines in the January 20, 2007 spectrum of NCyg06 that could be used to measure its abundance.

Iron is not enhanced. Because it is not produced by the nuclear reactions, it is expected to reflect the metallicity of the donor star, which should be around solar given the likely association of NCyg06 with the galactic disk at $R = 11.4$ kpc galactocentric distance.

The large overabundances of Ne observed in the spectra of some of the fastest novae are ascribed to mixing into the accreted envelope of material from the underlying white dwarf (e.g. Gil-Pons et al. 2003). In massive progenitors, non-degenerate carbon ignition leads to the formation of a degenerate core mainly made of oxygen and neon. The minimum mass on the zero age main sequence leading to extensive carbon-burning is $M \sim 9.3\ M_\odot$ and the resulting white dwarf will have a mass of $M_{\rm WD} \geq 1.1\ M_\odot$. Neon is not enhanced in NCyg06, in agreement with the above estimate of the white dwarf mass, which is below the limit for the ONe type.

12. Energy budget

The total energy budget of the outburst is the sum of the energy radiated from the central star and the binding and kinetic energy of the ejecta.

The energy radiated by the central star was computed by integrating the bolometric luminosity over time. For a rough order of magnitude estimate, we assumed that the $M_{\rm bol} = -8.0$ value at maximum declined linearly with time to $M_{\rm bol} = -6.45$ on $\Delta t = +290^d$, remaining there until the end of our observing campaign on $\Delta t = +530^d$. The result is

$$E_{\rm rad} = \int_0^{530} M_{\rm bol}(t) {\rm d}t = 1 \times 10^{46}\ {\rm erg}. \quad (11)$$

The actual time evolution of the bolometric luminosity is hard to define. Before NCyg06 settled to the constant luminosity phase, represented by $M_{\rm bol} = -6.45$ on $\Delta t = +290^d$, it went through a short-lived, super-Eddington phase characterized by $M_{\rm bol} = -8.0$ at peak V-band brightness. This is a common feature of observed novae and theoretical models (e.g. Starrfield 1989). Contrary to most novae, NCyg06 went through a second maximum, and this could have been reflected in an increase in $M_{\rm bol}$ above its plateau level. Thus a linear trend in luminosity evolution is adequate to derive an order of magnitude for the radiated energy, which is moreover a marginal term in the overall energy budget.

The kinetic energy of the ejected shell is

$$E_{\rm kin} = \frac{\xi}{0.43} \int_{r_{\rm in}}^{r_{\rm out}} 2\pi r^2 \rho(r) \left(\frac{r}{t}\right)^2 {\rm d}r = 2.2 \times 10^{47}\ {\rm erg} \quad (12)$$

where $\rho(r) = \rho(r_{\rm in})(r/r_{\rm in})^{-2}$ and the velocity of the ejecta is taken to be $v(r) = r/t$ which is consistent with an ejection over a short period of time around $t = 0$.

The outburst also had to provide the energy required to gravitationally unbound the ejected material. The binding energy depends from the mass of the white dwarf (its potential well). The binding energy of the above estimated $M^{\rm total}_{\rm ejected} = 4 \times 10^{-4}\ M_\odot$ from a $1.03\ M_\odot$ white dwarf is

$$E_{\rm bin} = 2 \times 10^{47}\ {\rm erg} \quad (13)$$

which is quite similar to the kinetic energy. As is typical of novae, most of the outburst energy goes into the mechanical work

of mass ejection, and only a few percent makes up the radiated fraction.

The total energy released by the outburst is therefore

$$E^{\rm tot} = E_{\rm bin} + E_{\rm rad} + E_{\rm kin} = 4.3 \times 10^{47} \ \ {\rm erg} \qquad (14)$$

which corresponds to the hydrogen burning of $4.6 \times 10^{-5}\ M_{\odot}$ of accreted material of solar composition, which is about 10% of the amount of mass accreted by the white dwarf prior to the outburst.

References

Arkhipova, V. P., Burlak, M. A., & Esipov, V. F. 2002, Astron. Lett., 28, 100
Bhatia, A. K., & Kastner, S. O. 1995, ApJS, 96, 325
Bonifacio, P., Selvelli, P. L., & Caffau, E. 2000, A&A, 356, L53
Bowen, I. 1947, PASP, 59, 196
Brand, J., & Blitz, L. 1993, A&A, 275, 67
Buscombe, W., & de Vaucouleurs, G. 1955, Obs., 75, 170
Cannizzo, J. K., & Mattei, J. A. 1992, ApJ, 401, 642
Capaccioli, M., della Valle, M., d'Onofrio, M., & Rosino, L. 1989, AJ, 97, 1622
Cohen, J. G. 1985, ApJ, 292, 90
Cohen, J. G. 1988, ASP Conf. Ser., 4, 114
Dehnen, W., & Binney, J. J. 1998, MNRAS, 298, 387
della Valle, M., & Livio, M. 1995, ApJ, 452, 704
de Vaucouleurs, G. 1978, ApJ, 223, 351
Dobrotka, A., Friedjung, M., Retter, A., Hric, L., & Novak, R. 2006, A&A, 448, 1107
Drilling, J. S., & Landolt, A. U. 2000, in Allen's Astrophysical Quantities, ed. A. N. Cox (Springer), 381
Evans, A., Geballe, T. R., Rawlings, J. M. C., Eyres, S. P. S., & Davies, J. K. 1997, MNRAS, 292, 192
Ferland, G. J., Korista, K. T., Verner, D. A., et al. 1998, PASP, 110, 761
Fitzgerald, M. P. 1970, A&A, 4, 234
Frigo, A., et al. 2006, IBVS, 5711
Gallagher, J. S. 1977, AJ, 82, 209
Gallagher, J. S., & Starrfield, S. 1978, ARA&A, 16, 171
Gehrz, R. D. 1988, ARA&A, 26, 377
Gehrz, R. D. 1990, in Physics of Classical Novae, ed. A. Cassatella, & R. Viotti, IAU Coll., 122 (Springer-Verlag), Lecture Notes in Physics, 369, 138
Gehrz, R. D. 2002, in Classical Nova Explosions, ed. M. Hernanz, & J. José, AIP Conf. Proc., 637, 198
Gehrz, R. D., Greenhouse, M. A., Hayward, T. L., Houck, J. R., et al. 1995, ApJ, 448, L119
Gehrz, R. D., Truran, J. W., Williams, R. E., & Starrfield, S. 1998, PASP, 110, 3
Gil-Pons, P., Garci'a-Berro, E., José, J., Hernanz, M., & Truran, J. W. 2003, A&A, 407, 1021
Goranskij, P. V., Metlova, V. N., & Burenkov, N. A. 2006, ATel, 928
Herbig, G. H. 1995, ARA&A, 33, 19
Hernanz, M. 2005, in The Astrophysics of Cataclysmic Variables and Related Objects, ed. J.-M. Hameury, & J.-P. Lasota, ASP Conf. Ser., 330, 265
Hron, J. 1987, A&A, 176, 34
Isobe, S., Sasaki, G., Norimoto, Y., & Takahashi, J. 1986, PASJ, 38, 511
Jurdana-Sepič, R., & Munari, U. 2006, IBVS, 5738
Kastner, S. O., & Bhatia, A. K. 1995, ApJ, 439, 346
Kimeswenger, S., Dalnodar, S., Knapp, A., et al. 2008, A&A, 479, L51
Kiyota, S., Kato, T., & Yamaoka, H. 2004, PASJ, 56, 193
Livingston, W. C. 2000, in Allen's Astrophysical Quantities, 4th edn., ed. A. N. Cox (Springer), 339
Lynch, D. K., et al. 2006, IAUC, 8784
Mason, C. G., Gehrz, R. D., Woodward, C. E., et al. 1996, ApJ, 470, 577
Mazuk, S., et al. 2006, IAUC, 8730
McLaughlin, D. B. 1960, in Stellar Atmospheres, ed. J. L. Greenstein (Univ. Chicago Press), 585 (McL60)
Megier, A., Krelowski, J., & Weselak, T. 2005, MNRAS, 358, 563
Mobberley, M. 1999, JBAA, 109, 57
Munari, U., & Zwitter, T. 1997, A&A, 318, 269
Nakano, S. 2006, IAUC, 8697
Neckel, Th., & Klare, G. 1980, A&AS, 42, 251
Osterbrock, D. E. 1989, Astrophysics of Gaseous Nebulae and Active Galactic Nuclei (Univ. Science Books)
Payne-Gaposchkin, C. 1957, The Galactic Novae (North-Holland) (PG57)
Pfau, W. 1976, A&A, 50, 113
Prialnik, D. 1990, in Physics of Classical Novae, ed. A. Cassatella, & R. Viotti, IAU Coll. 122 (Springer-Verlag), Lect. Notes Phys., 369, 351
Rayner, J., et al. 2006, IAUC, 8787
Russell, R. W., Rudy, R. J., Lynch, D. K., & Woodward, C. E. 2006, IAUC, 8709
Schmidt, T. 1957, ZA, 41, 182
Shore, S. N., & Gehrz, R. D. 2004, A&A, 417, 695
Starrfield, S. 1989, in Classical Novae, ed. M. F. Bode, & A. Evans (John Wiley & Sons publisher), 39
Steeghs, D., et al. 2006, ATel, 795
Strittmatter, P. A., Woolf, N. J., Thompson, R. I., et al. 1977, ApJ, 216, 23
Tomov, T., Moro, D., & Munari, U. 1999, IAUC, 7225
Vallée, J. P. 2005, AJ, 130, 569
van den Bergh, S. 1988, PASP, 100, 8
van den Bergh, S., & Younger, P. F. 1987, A&AS, 70, 125
Venturini, C. C., Rudy, R. J., Lynch, D. K., Mazuk, S., Puetter, R. C., et al. 2004, AJ, 128, 405
Wallace, P. 1994, in Astronomical Data Analysis Software and Systems III, ed. D. R. Crabtree, R. J. Hanisch, & J. Barnes, ASP Conf. Ser., 61, 481
Warner, B. 1995, Cataclysmic Variable Stars (Cambridge Univ. Press)
Williams, R. E. 1992, AJ, 104, 725
Williams, R. E. 1994, ApJ, 426, 279
Yamaoka, H. 2006a, IAUC, 8698
Yamaoka, H. 2006b, IAUC, 8702
Zwitter, T., & Munari, U. 1995, A&AS, 114, 575

Table 3. Photometry of the progenitor of Nova Cyg 2006 on photographic plates of the Asiago Schmidt Telescopes archive. This material is new and extends the coverage in time of the 1962−1984 archive material presented by Jurdana-Sepič & Munari (2006). The nova progenitor is always below the plate magnitude limit, which is given in column seven, with respect to the photometric sequence calibrated by Frigo et al. (2006).

yy	mm	dd	UT (hh:mm)	expt (min)	band	mag	emulsion type	filter	plate ident
1989	8	2	00:45	30	I	>16.29	IN	RG 5	SG14580
1989	10	6	23:38	30	I	>16.14	IN	RG 8	SG14639
1989	10	25	20:03	30	B	>18.10	103a O	GG 13	SG14657
1989	10	25	20:50	30	I	>16.29	IN	RG 8	SG14658
1989	11	29	19:55	30	B	>18.10	103a O	GG 13	SG14719
1989	11	29	20:35	30	I	>16.14	IN	RG 8	SG14720
1990	7	27	23:06	30	B	>18.10	103a O	GG 13	SG14810
1990	7	27	23:50	30	I	>16.29	IN	RG 8	SG14811
1990	8	23	23:46	30	B	>18.60	103a O	GG 13	SG14859
1990	8	26	00:35	30	I	>16.14	INsen	RG 8	SG14870
1990	10	22	19:56	30	B	>18.60	103a O	GG 13	SG14903
1990	10	22	20:47	30	I	>16.29	INsen	RG 8	SG14904
1991	11	7	21:13	30	B	>18.10	103a O	GG 13	SG15062
1991	11	7	21:54	30	I	>16.29	INsen	RG 8	SG15063
1991	11	30	21:51	30	B	>18.60	103a O	GG 13	SG15072
1991	11	30	22:43	30	I	>15.89	INsen	RG 8	SG15073
1991	12	2	21:58	30	B	>18.60	103a O	GG 13	SG15083
1991	12	2	22:41	30	I	>16.29	INsen	RG 8	SG15084
1991	12	6	19:30	30	B	>18.60	103a O	GG 13	SG15106
1991	12	6	20:10	30	I	>16.29	INsen	RG 8	SG15107
1992	7	2	23:51	30	I	>16.29	INsen	RG 8	SG15252
1992	8	27	22:55	30	B	>18.60	103a O	GG 13	SG15271
1992	9	25	23:20	30	B	>18.60	103a O	GG 13	SG15290
1992	9	26	00:01	30	I	>16.29	INsen	RG 8	SG15291
1992	10	20	23:01	30	B	>18.60	103a O	GG 13	SG15301
1992	10	21	00:43	30	I	>15.89	INsen	RG 8	SG15302
1992	10	24	20:53	30	B	>18.60	103a O	GG 13	SG15304
1992	10	24	21:39	31	I	>16.29	INsen	RG 8	SG15305
1992	12	18	18:59	30	B	>18.60	103a O	GG 13	SG15341
1992	12	18	19:44	30	I	>16.29	INsen	RG 8	SG15342
1993	7	06	23:53	08	B	>18.10	103a O	GG 13	SG15578
1993	7	7	00:10	08	I	>15.04	INsen	RG 8	SG15579
1993	8	15	22:53	30	I	>16.29	INsen	RG 8	SG15607
1993	8	15	23:33	30	B	>18.60	103a O	GG 13	SG15608
1993	8	19	23:38	30	B	>18.60	103a O	GG 13	SG15620
1993	8	20	00:20	30	I	>16.29	IN	RG 8	SG15621
1993	9	10	21:53	30	B	>18.60	103a O	GG 13	SG15641
1993	9	10	22:42	30	I	>16.29	IN	RG 8	SG15642
1993	10	19	21:52	30	B	>18.10	103a O	GG 13	SG15657
1993	11	18	20:56	30	B	>18.60	103a O	GG 13	SG15671
1993	11	18	21:36	30	I	>16.29	IN	RG 8	SG15672
1993	12	9	20:22	30	B	>18.10	103a O	GG 13	SG15684
1993	12	9	21:13	30	I	>16.29	IN	RG 8	SG15685
1993	12	10	21: 0	20	B	>18.60	103a O	GG 13	SG15690
1994	8	12	21:02	15	B	>18.10	103a O	GG 13	SG15786
1994	11	28	21:03	20	B	>18.60	103a O	GG 13	SG15821
1996	7	10	00:44	30	B	>18.60	103a O	GG 13	SG16124
1996	7	11	01:46	30	I	>16.14	IN	RG 8	SG16125
1996	9	8	00:33	30	B	>18.60	103a O	GG 13	SG16147
1996	9	8	01:54	30	I	>16.29	IN	RG 8	SG16148
1996	10	4	20:17	30	I	>16.29	IN	RG 8	SG16158
1996	11	4	18:45	30	B	>18.60	103a O	GG 13	SG16166
1996	11	4	19:54	30	I	>16.29	IN	RG 8	SG16167
1996	11	8	19:30	30	B	>18.60	103a O	GG 13	SG16175
1997	9	24	22:02	30	I	>16.29	IN	RG 8	SG16493
1997	10	1	21:49	30	B	>18.60	103a O	GG 13	SG16507
1997	10	1	22:30	30	I	>16.29	IN	RG 8	SG16508

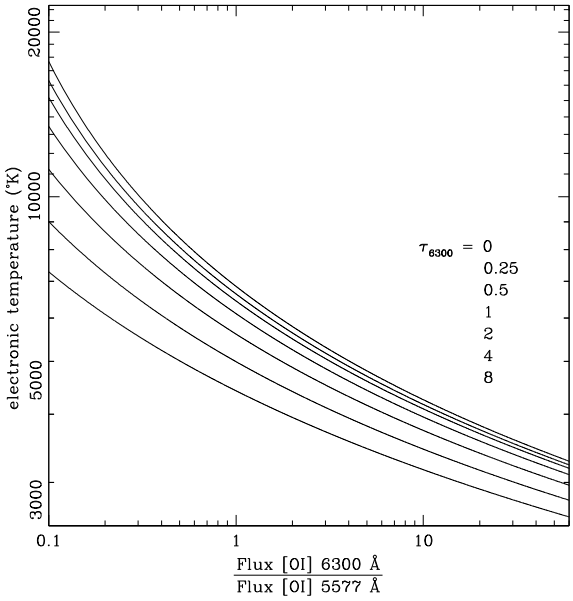

Fig. 7. Electron temperature as a function of (reddening corrected) [OI] 6300/[OI] 5577 flux ratio for different values of optical depth in the 6300 line.

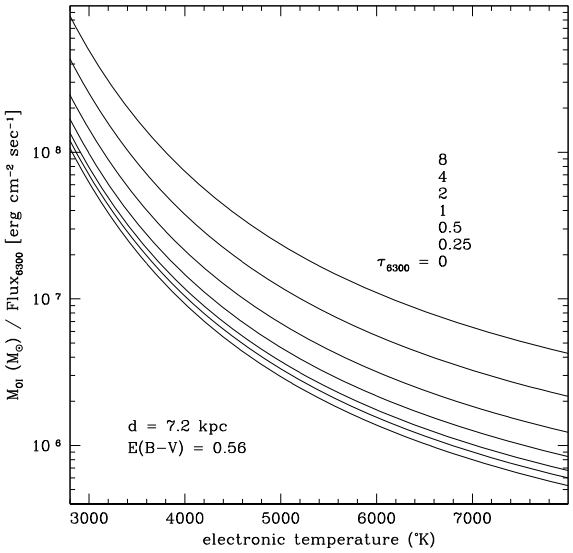

Fig. 8. Ratio between mass of neutral oxygen in the ejecta and [OI] 6300 line flux as a function of [OI] 6300 emission line optical depth, at 7.2 kpc distance and $E_{B-V} = 0.56$ estimated for Nova Cyg 2006.

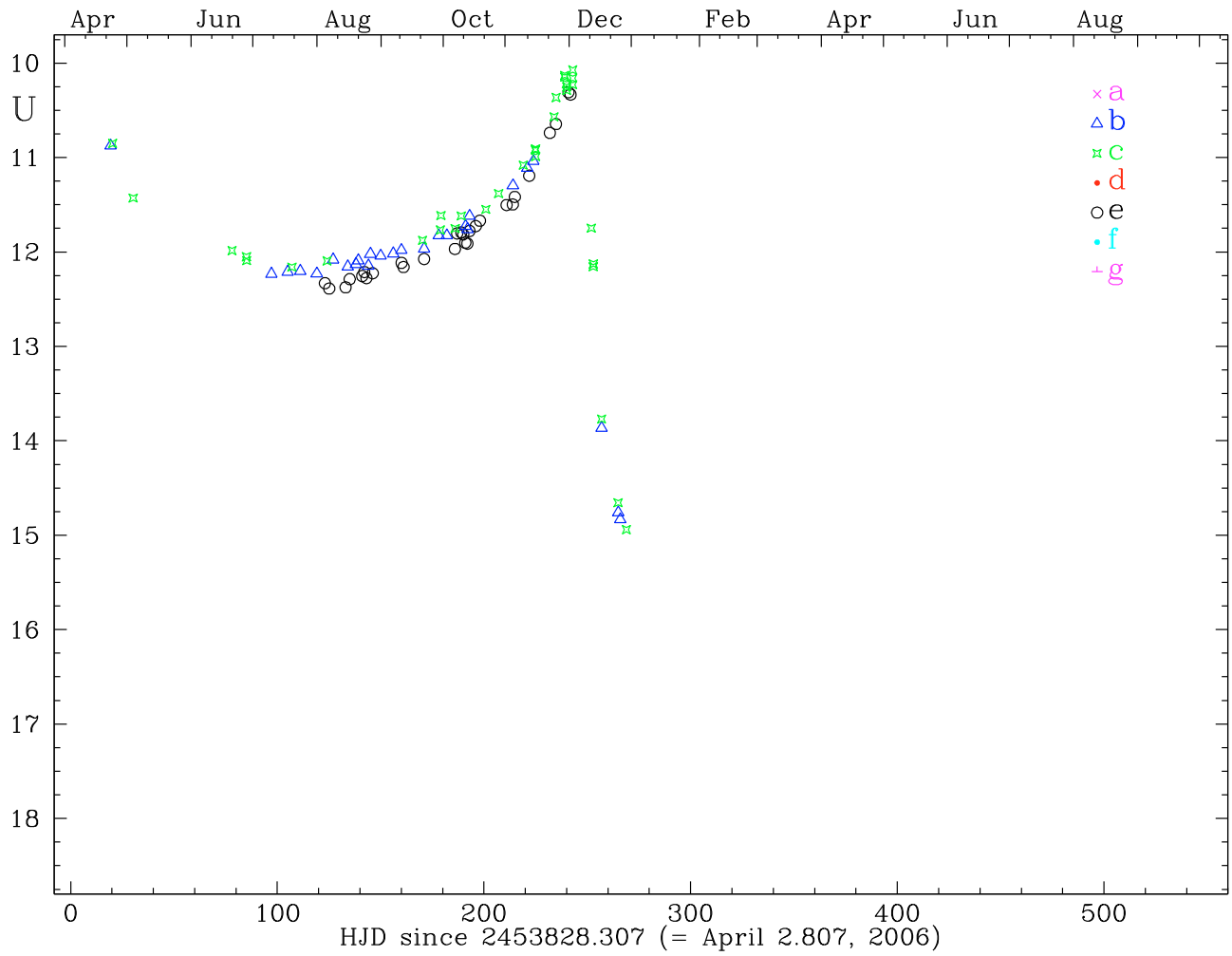

Fig. 16. *U*-band lightcurve of Nova Cyg 2006 formed with all data available in Table 1, color- and symbol-coded according to the different instruments that collected the data (see Sect. 2.1 for *a-g* instrument identification letters).

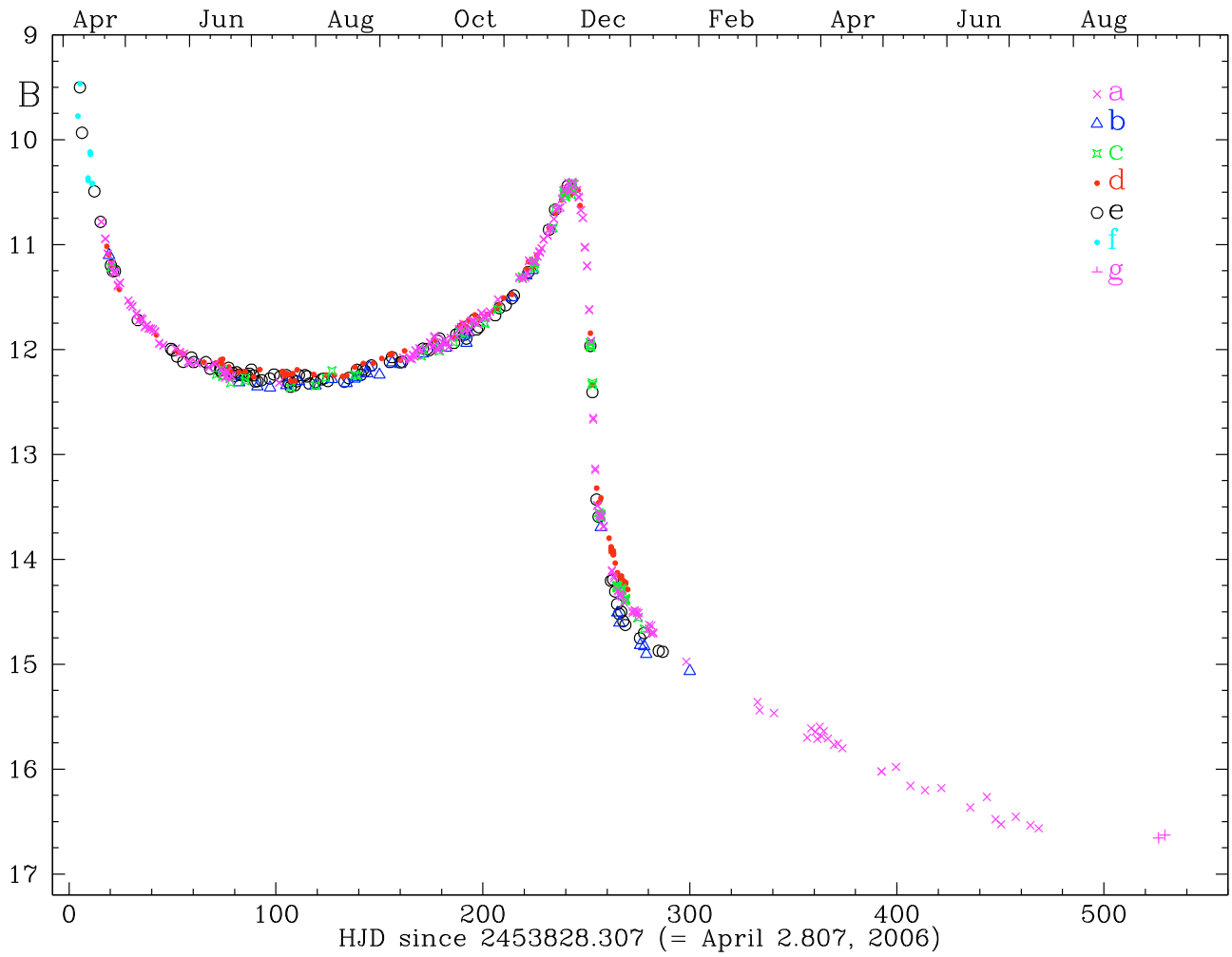

Fig. 17. *B*-band lightcurve of Nova Cyg 2006 formed with all data available in Table 1, color- and symbol-coded according to the different instruments that collected the data (see Sect. 2.1 for *a-g* instrument identification letters).

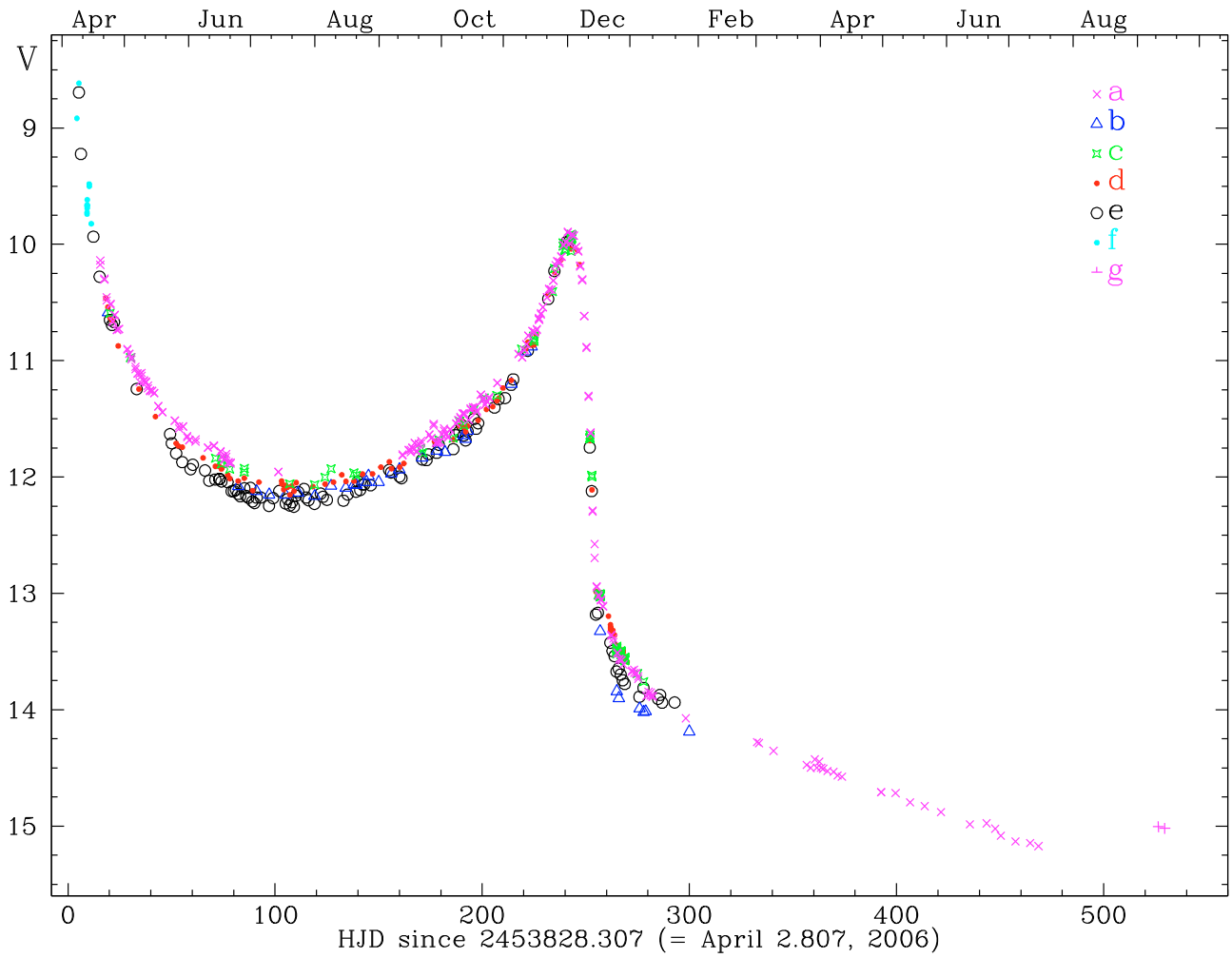

Fig. 18. *V*-band lightcurve of Nova Cyg 2006 formed with all data available in Table 1, color- and symbol-coded according to the different instruments that collected the data (see Sect. 2.1 for *a-g* instrument identification letters).

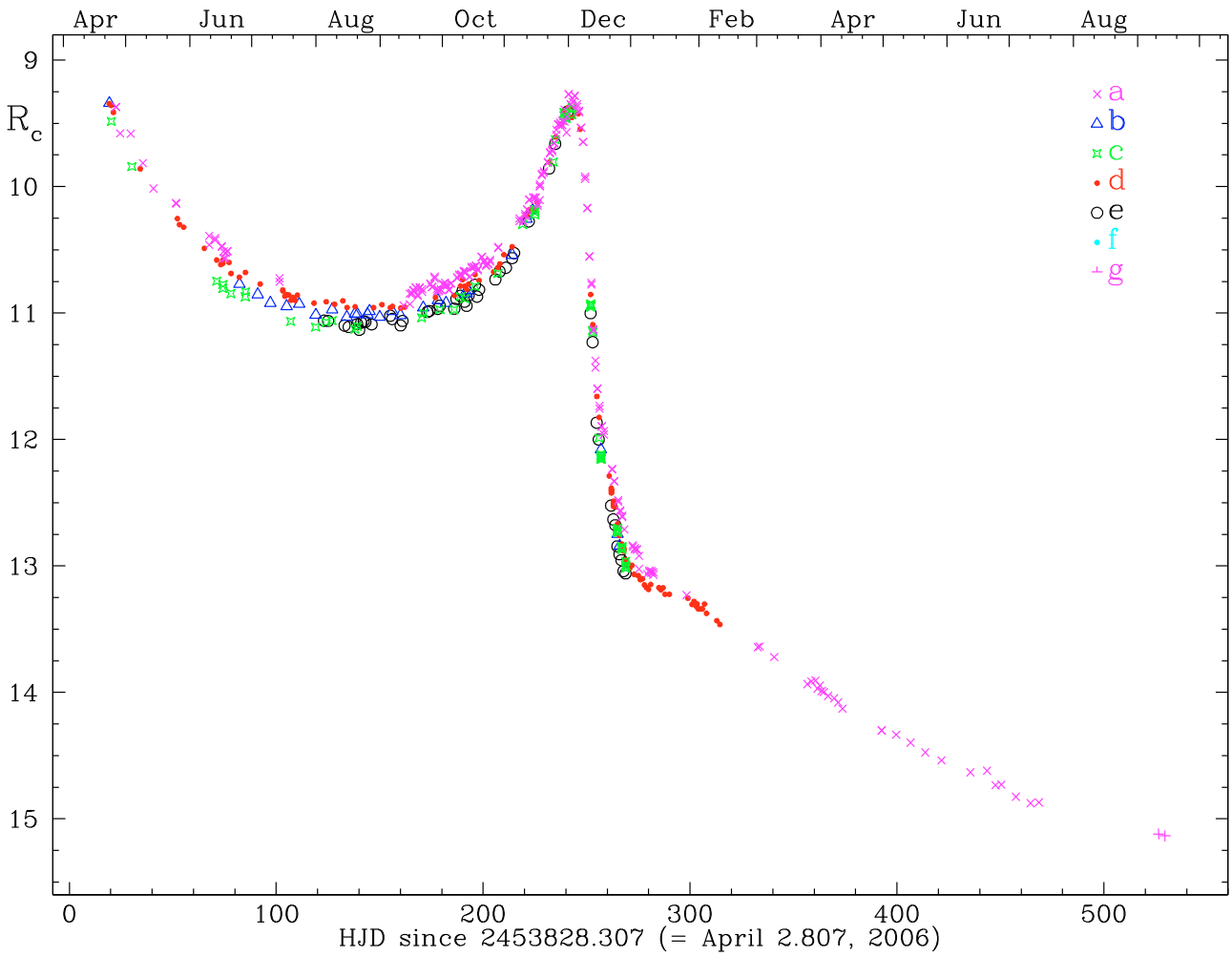

Fig. 19. R_C-band lightcurve of Nova Cyg 2006 formed with all data available in Table 1, color- and symbol-coded according to the different instruments that collected the data (see Sect. 2.1 for *a-g* instrument identification letters).

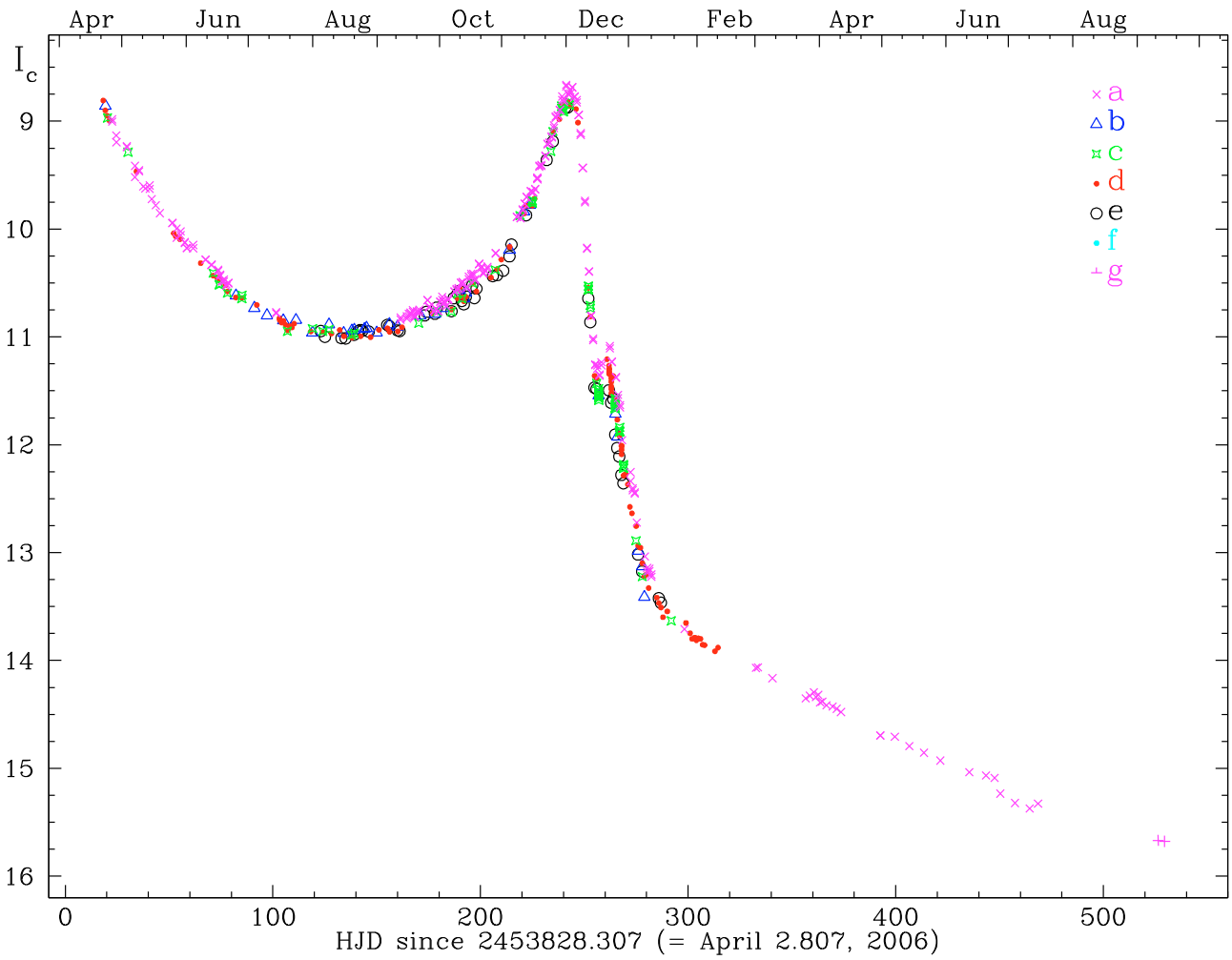

Fig. 20. I_C-band lightcurve of Nova Cyg 2006 formed with all data available in Table 1, color- and symbol-coded according to the different instruments that collected the data (see Sect. 2.1 for *a-g* instrument identification letters).